NATIONAL ADVISORY COMMITTEE FOR AERONAUTICS

TECHNICAL NOTE

No. 988

STRENGTH OF WING BEAMS UNDER AXIAL AND TRANSVERSE LOADS

By Walter Ramberg, A. E. McPherson, and Samuel Levy
National Bureau of Standards

Washington
September 1945

NATIONAL ADVISORY COMMITTEE FOR AERONAUTICS

TECHNICAL NOTE NO. 988

STRENGTH OF WING BEAMS UNDER AXIAL AND TRANSVERSE LOADS

By Walter Ramberg, A. E. McPherson, and Samuel Levy

SUMMARY

Wing beams of six designs (figs. 1a to 1f), referred to as types A to F, were tested under axial compressive loads, transverse loads, and combined axial and transverse loads. Type A was a stainless-steel box beam, types B and C were 17S-T and 24S-T aluminum-alloy I-beams with parallel flanges, type D was a 24S-T aluminum-alloy I-beam with curved flanges, type E was a 17S-T aluminum-alloy I-beam with tilted flanges, and type F was an AM59S-T magnesium-alloy I-beam with parallel flanges. Two specimens of each type were loaded in compression only. Four specimens of each type were loaded by combined axial and transverse load with the location of the load points so chosen as to produce failure in the central portion of the beam. The remaining two specimens of each type were loaded by transverse loads alone with the moment arms of the transverse loads so chosen as to produce failure by bending in the central portion for one specimen and by shear in the end portions for the other.

Deflections and strains in the elastic range were in general agreement with those computed from the simple beam theory after taking account of the secondary bending moment produced by the axial load as the beam deflected under load.

Failure of all I-beams except some of those tested in shear was due to local instability of the compression flange with extreme fiber stress at failure increasing as the ratio of bending moment to axial load increased. Both bending moment at failure and axial load at failure decreased rapidly with increasing length for beams A, D, and E; there was very little length effect in the case of beams B, C, and F.

The interaction curves for combinations of axial load and bending moment could be approximated by straight lines. A procedure is given for estimating the strength under combined axial and transverse loads of beams similar to those

that were tested from the strengths under axial load and transverse load acting separately. The computed values so obtained for combined axial and transverse loads were from 11 percent smaller to 14 percent larger than the corresponding measured values.

Comparison of the strength-weight ratios shows that types D and F having relatively compact sections were superior to the others in their ability to resist compression, bending moment, and transverse shear. Comparison of the stiffness-weight ratios shows that types B, C, and E having relatively thin-walled sections were stiffest although type F, having a compact section, had a stiffness-weight ratio only 15 percent below the highest value, which was obtained for type C.

INTRODUCTION

The tests of wing beams described in this paper form a portion of a research program conducted by the National Bureau of Standards for the Bureau of Aeronautics, Navy Department, from 1933 to 1944. The purpose of this program was to gather data on the ultimate strength and deformation of wing beams of a number of typical designs.

NOTATION

E	Young's modulus (lb/in.^{2})
$G = \frac{E}{2(1+\mu)}$	shear modulus (lb/in.^{2})
μ	Poisson's ratio (0.3)
I	maximum principal moment of inertia of cross section (in.^{4})
A	cross-sectional area (in.^{2})
k/AG	change in slope of deflection curve, dy/dx, due to a transverse shearing force of 1 pound (lb^{-1})
x	coordinate in axial direction (in.)
y	coordinate in transverse direction (in.)

l length of beam between hinge points at ends; half-length for beams loaded in axial compression with flat ends (in.)

e eccentricity of axial load relative to center of gravity of section (in.)

a distance of each transverse load point from nearer hinge point at end (in.)

c distance from neutral axis to extreme fiber (in.)

P_c axial compressive load (lb)

P_b transverse load applied at each intermediate load point ($2P_b$ = total transverse load) (lb)

M_b bending moment due to transverse loads only (lb-in.)

w weight of beam per unit length (lb/in.)

δ_c deflection at center of beam (in.)

f_c axial compressive stress (lb/in.^{2})

f_b extreme fiber bending stress (lb/in.^{2})

$f_t = f_c + f_b$ total extreme fiber stress (lb/in.^{2})

DESCRIPTION OF WING BEAMS

Dimensions

Tests were made on beams of six different designs referred to in the following paragraphs as types A to F. Cross-sectional dimensions for the six types and details of stiffener design are given in figures 1a to 1f.

Type A was an 18-8 stainless-steel box beam assembled by spot-welding formed sheet into the section shown in figure 1a. The beam was reinforced at intervals of about $2\frac{1}{2}$ inches by channel-type stiffeners spot-welded to the web.

Type B was a 17S-T aluminum-alloy I-beam with straight flanges (fig. 1b). The beam was assembled by riveting two

extruded T-bar cap-strips to the web of the beam. The web was stiffened by channel-type stiffeners spaced 3.5 inches between centers.

Type C (fig. 1c) was identical with type B, except for the use of 24S-T aluminum alloy in place of 17S-T aluminum alloy.

Type D was a 24S-T aluminum-alloy I-beam with curved flanges (fig. 1d). The beam was assembled by riveting two cap-strips to a web which fitted into a slot in the leg of each cap-strip. There were no stiffeners on the web of the beam.

Type E was a 17S-T aluminum-alloy I-beam with tilted flanges (fig. 1e). The beam was stiffened by stiffeners riveted to one side of the web and to the cap-strips at intervals of about 10 inches.

Type F was an extruded AM59S-T magnesium-alloy I-beam with parallel flanges, die M704 (K-8665), (fig. 1f). There were no stiffeners on the web of the beam.

Cross-sectional areas and maximum principal moments of inertia were determined from the measured dimensions of a number of specimens of each type with the results given in tables 1A to 1F. The lengths of the individual specimens, the weights per unit length, and the slenderness ratios are also given in tables 1A to 1F.

Load

Eight specimens of each type were tested as indicated:

Specimen 1	short column
Specimen 2	long column
Specimen 3	short beam under combined (predominantly axial) load
Specimen 4	long beam under combined (predominantly axial) load
Specimen 5	short beam under combined (predominantly transverse) load

Specimen 6 long beam under combined (predominantly transverse) load

Specimen 7 beam under transverse (predominantly bending) load

Specimen 8 beam under transverse (predominantly shearing) load

The proportions of axial and transverse loads were varied to determine the effect of changes in the ratio of extreme fiber bending stress to total stress. The initial value of this ratio is given as $n = f_b/f_t$ in tables 1A to 1F. The ratio was increased in approximately equal steps from 0 for the column specimens 1 and 2, to 1 for the specimens under transverse load, 7 and 8. Two lengths of column specimen and two lengths for each combination of axial and transverse load were included to give an indication of the effect of changes in length.

Tensile and Compressive Properties of Material

No material was available for tensile and compressive tests of the sheet in specimens A. An approximate, partial, description of the compressive stress-strain curve was obtained from the test of the short column specimen 1A by plotting average stress against average strain (fig. 2a). The plot indicates a Young's modulus of about 27.3×10^6 pounds per square inch. Tensile properties of flange and web material of the beams of types B to F were determined on standard specimens (reference 1) with the use of 2-inch Tuckerman optical strain gages for measuring strains. The results are given in figures 2b to 2f and in table 2. Compressive properties of the flange materials of beams B to F were obtained by pack tests (reference 2) with results given also in figures 2b to 2f and in table 2.

The material appeared to be homogeneous in properties except for beams of type E. For these beams the material showed segregation into high-strength and low-strength flange material as brought out by figure 2e. Polished and etched transverse sections showed that the low-strength material was composed of very large crystals while the high-strength material had the usual appearance. The large grain size was ascribed to abnormal grain growth during fabrication or heat treatment.

The tensile yield strengths for the material in beams B to E were from 9 to 20 percent greater than the compressive yield strengths of the same material. For beams F the yield strengths were nearly the same in tension and compression. The values of Young's modulus in compression for the materials in beams B to F were from 1 to 5 percent greater than the values in tension. Elongations ranged from 9 to 25 percent in 2 inches.

TESTS

The test procedure was changed as improvements in technique were made during the long interval covered by the tests.

Specimens under Axial Load

Test procedure.- Three kinds of end conditions were used in the column tests. Specimens 1A and 1F were tested between flat ends as shown in figure 3; specimens, 1B, 1C, 1D, 2A, 2B, 2C, and 2D were tested between ball-bearing "pin ends" as shown at A in figure 4; and specimens 1E, 2E, and 2F were tested between knife-edge pin ends as shown at A in figures 5 and 6. The equivalent length l of the columns was taken as half the length between flats in the flat-end tests and the full length between axes of rotation in the pin-end tests. For all the specimens except 2A, for which no strain gage measurements were made, the individual strains at the ends as measured with four Tuckerman strain gages were within 10 percent of their average value.

Lateral guides were used for all long specimens and the short specimen, 1E, to prevent buckling about the axis of least stiffness. A "ball type" of guide shown at B in figures 4, 6, and 7 was used in testing specimens 1E, 2B, 2C, 2D, and 2E. This guide had a coefficient of friction of only 0.02 for motions parallel to the web and was essentially rigid in a direction perpendicular to the web. A "cage type" of guide shown at B in figure 5 was used in testing specimen 2F. This guide could be moved on the specimen at all loads without binding. A guide consisting of angle irons clamped to a channel was used in the test of specimen 2A. No guide was used in the tests of the relatively short specimens, 1A, 1B, 1C, 1D, and 1F as it was expected that these specimens would fail by local instability before column failure about the axis of minimum moment of inertia.

The strain at the middle portion of the specimen was measured with four Tuckerman strain gages, except in the case of specimen 2A. These gages are shown at A on figure 3 and at C on figures 4, 6, and 7.

Results of axial load tests.- The loads, average stresses at failure, and the type of failure are given in the summary tables 3A to 3F. The type of failure is also apparent from the photographs of specimens after test (figs. 8a to 8f).

Average-stress values were obtained from the strain-gage readings made in the tests of beams of types B to F by converting each individual strain into stress with the help of the compressive stress-strain curve of the material (figs. 2b to 2f). In the case of specimens of type A, no stress-strain curve of the material other than the test of specimen 1A was available; so no comparison was possible. The average stress for specimens of types B to F is compared with the average stress P/A, obtained by dividing the load by the original area, in figures 9a to 9e. The average axial stress in the flanges, as measured by the gages, was equal to the computed average stress P/A up to a certain critical value which ranged from about 6000 lb/in.^{2} for the specimen of types B and C to about 20,000 lb/in.^{2} for the specimens of type D. These critical stresses corresponded roughly to the stresses at which buckles were first observed in the webs of the specimens. The increase in average flange stress above the critical stress is attributed to a decrease in the load-carrying capacity of the web after buckling.

Theoretical values for the increase in flange stress due to buckling of the web are shown as dotted curves in figures 9a to 9e. The upper dotted curve assumes that the web is rigidly clamped at the flanges, while the lower curve assumes simple support at the flanges. The actual restraint is between these two extremes.

The curves for figures 9a and 9b (close spacing of transverse stiffeners) were computed on the assumption that the load after buckling is given by Marguerre's approximate formula (reference 3):

$$\frac{w_e}{w_o} = \sqrt[3]{\frac{\epsilon_{cr}}{\epsilon}} \qquad (1)$$

where

w_e/w_o ratio of effective width to initial width of web between flanges

ϵ/ϵ_{cr} ratio of strain in flanges to critical strain for buckling of web

This formula was used since no specific solution is available for a web having closely spaced transverse stiffeners. The curves for figures 9c, 9d, and 9e (wide spacing of transverse stiffeners) were computed by replacing the full width of the web by an effective width the variation of which with the axial stress was computed from theoretical solutions for the buckling of a plate without transverse stiffeners (fig. 5 of reference 4 and fig. 8 of reference 5).

The observed points fall between the theoretical curves within the error of observation, except, that at high loads, yielding of the material causes the points for specimens 2B and 2E to fall below the lower of the two theoretical curves.

Visual examination of specimen 2A showed bending about the axis of least stiffness. Examination of strain readings at the flanges for specimens 1B, 1C, 1D, 2D, 1E, and 2E indicated either twisting of the flanges toward each other or appreciable bending about the axis of least stiffness. Bending about the axis of least stiffness may have resulted in a reduction of the load at failure. An estimate of the load at failure which would have been attained in the absence of this bending was derived from the tests under combined load (see section under Effect of Length on Loads at Failure for Column Specimens 1 and 2). The values for beams 1B, 1C, 1D, 2D, 1E, and 2E are given in parentheses in tables 3B to 3E; no estimate could be obtained in the case of beam 2A since strains were not measured on the combined load specimens 3A to 6A.

Examination of the specimens after failure (figs. 8a to 8f) shows that the final failure of the box beams A was by local buckling of web and flanges, while that for the I-beams B to F was by local buckling of the flanges.

In view of the small effect of length on the load at failure indicated by a comparison of results for specimens 1 and 2 of types B to F, it is probable that this local buckling was the primary cause of failure in all column specimens with an I-section.

Tests under Combined Axial and Transverse Loads

Test procedure.- Loads were applied to the specimens by two different machines. The machine shown in figure 10 was used in testing all the combined load specimens of types A, B, and C and specimens 4D and 6D. End loads were applied to the specimen A with the hydraulic jacks B at a small angle with the axis of the beam. The vertical component of these end loads was reacted by the tension members C. The axial and transverse loads were computed from the measured load on the platform scale D and the geometry of the system. The effect of friction at the bearing E between the jack carriage and its support was minimized in all tests except that of specimen 4C by moving the carriage to equilibrium by hand. The load measuring system was checked by a proving ring and found to measure axial loads within 0.5 percent. No check was made on the accuracy of measuring transverse loads. The fixture shown in figure 11 was used in testing all the combined load specimens of types E and F and specimens 3D and 5D. The fixture applied end loads and transverse loads to the specimen A at B and C, respectively, by the built-up angles D. These angles were in turn loaded at points E by the testing machine F. The line of loading of the angles was displaced a short distance from the center line of the beam, and the moment on the angles resulting from this eccentricity of axial load was counteracted by the tension on the pull-rods C and a transverse shear at B. Thin flexure rods were used to float the fixture in a horizontal plane to prevent loading of the specimen by the dead weight of the fixture. This dead weight was approximately 1600 pounds. The accuracy of measurement of both the axial and transverse loads was within the accuracy of the testing machine (error less than 1 percent).

The ends of the specimens of types A, B, and C and of specimens 4D and 6D were loaded through ball-bearing pin ends as shown at F on figure 10. The ends of the specimens of types E and F and of specimens 3D and 5D were loaded through knife-edge pin ends.

Lateral guides were used in the tests to prevent buckling about the axis of minimum stiffness. The "iron-bar type" of guide shown at G in figure 10 was used in testing all the specimens of types A, B, and C and specimens 4D and 6D. This guide was adjusted during test barely to make contact with the specimen. The ball type of guide shown at B in figures 4, 6, and 7 was used in testing all the specimens of type E and specimens 3D and 5D. The cage type of guide shown at B in figure 5 was used in testing all specimens of type F.

Deflections due to bending were measured from a reference system connected to the heads of the specimen. In the case of specimens of types A, B, and C and of specimens 4D and 6D deflections were measured to the nearest 0.01 inch from a taut wire. For the remaining specimens the deflections were measured to the nearest 0.001 inch from a strain-free reference bar. The measured deflections were corrected to give the deflections relative to a line connecting the pin ends.

Strain was measured near the center of the specimens of types B, C, D, E, and F by one or two pairs of Tuckerman strain gages. No strains were measured on specimens of type A.

Results of combined load tests.- The measured center deflection of the beams under combined load is compared in figures 12a to 12f with the theoretical deflection computed from the formula

$$\delta_c = P_b \left[\frac{a}{24EI} (3l^2 - 4a^2) + \frac{b}{A_e G} \right] \Big/ \left(1 - \frac{P_c}{P_e} \right) \qquad (2)$$

where $P_b a (3l^2 - 4a^2)/24EI$ is the deflection due to bending alone, $P_b b/A_e G$ is the deflection due to shear alone, the factor $1/(1 - P_c/P_e)$ takes account of the approach of the axial load to the critical load, and

P_e Euler buckling load, taking account of shearing deformation (see p. 139 of reference 6)

$$= \frac{\pi^2 EI}{l^2} \Big/ \left(1 + \frac{1}{A_e G} \frac{\pi^2 EI}{l^2} \right)$$

$A_e = \frac{ht}{1.2}$ effective area subjected to uniform shear (see pp. 126, 127, and 189 of reference 7)

h web depth

t web thickness

b length of beam subjected to shear between loading head and transverse load point

The results, figures 12a to 12f, show that on the average the observed and calculated deflections agree for stresses in the elastic range; however, the scatter is very large. Even in the case of specimens of types B and E which showed the least scatter, the maximum difference for low stresses is 10 percent; while the maximim difference for specimens of type A, which showed the greatest scatter at low stresses, is 35 percent. This scatter is attributed to friction in the lateral guides and to friction in the test fixture shown in figure 10. Friction should be negligible in the fixture shown in figure 11.

The measured extreme fiber stresses f_{t_3} are compared in figures 13a to 13e with the theoretical values f_{t_1} obtained by substitution in the simple beam formula:

$$f_{t_1} = \frac{P_c}{A} + \frac{(M_b + P_c\delta_c)c}{I} \qquad (3)$$

where f_{t_1} is the extreme fiber stress at center of specimen. No comparison is given for specimens of type A or for specimen 4C since strain gages were not used in testing these specimens. The measured and calculated stresses for all specimens agreed within 10 percent for stresses below 20,000 lb/in^2. At stresses higher than this, buckling of the web caused the observed stresses to be larger than the calculated stresses for some of the specimens. The maximum difference was 18 percent for specimens 3B and 3C. Nölke (reference 8) found that the extreme fiber stress for buckling of a simply supported web in the elastic range increased 5.7 times in going from pure column loading ($n = 0$) to pure bending ($n = 1$). The specimens of types B, C, and F which showed signs of web buckling all buckled at stresses in the plastic range, so that no quantitative check of Nölke's theory could be made; however, the experimental results do check qualitatively in showing an increase in critical stress with increase in the ratio n of bending stress to total stress.

The axial loads, bending moments, center deflections, and extreme fiber stresses at failure are given in tables 3A to 3F. The types of failure are indicated in the last column of these tables and are shown in the photographs of specimens after test (figs. 8a to 8f). Failure was due to local instability of the flanges for all specimens under combined

axial and transverse load. Extreme fiber stresses at failure were computed by three methods:

1. The theoretical extreme fiber stress f_{t_1} was obtained from equation (3) with equation (2) used to compute δ_c.

2. The semiempirical extreme fiber stress f_{t_2} was obtained from equation (3) with the use of the observed value of δ_c.

3. The empirical extreme fiber stress f_{t_3} was obtained by converting readings of extreme fiber strain into stress with the use of the stress-strain curves given in figures 2b to 2f.

The stress at failure, according to all three methods of computing, shows a tendency to increase as the loading passes from axial to bending loads. This indicates greater stability of the compression flange under bending loads than under either combined or axial loads.

Beams under Transverse Loads

Test procedure.- Tests under transverse loads were made on specimens 7 and 8 of each type of wing beam. For specimens 7, the transverse load was applied at the third points so that the middle third of the beam was subjected to a constant bending moment. For specimens 8, the transverse load was applied at points close enough to the ends to make failure in shear in the outer portion more likely than failure by bending in the center portion. Specimen 8F failed in bending rather than shear in spite of this.

The method of applying transverse load to specimen 8F is shown in figure 14. The specimen A is loaded by pull-bars B in an upward direction and by pull-bars C in a downward direction. The outer portions D are subjected to combined bending and transverse shear, while the center portion is subjected to pure bending. The connections E were formed by pins fitting loosely in oversize holes. Equalizers F were used to apply load to the specimen symmetrically. The load was applied and measured by the testing machine G. The error of this machine was less than 1 percent.

Lateral guides to prevent tipping of the beam as a whole due to lateral instability were used in tests of specimens 7. These specimens were long enough to make restraint against lateral instability advisable. The guides were of the "angle-iron type" for tests of specimens 7A, 7B, 7C, 7D, and 7E, and of the cage type for test of specimen 7F. In all cases the guides were adjusted to barely touch the sides of the beam and to offer a minimum restraint to motion in the plane of the web.

Deflection of the specimen was measured by dial micrometers H with respect to the strain-free reference bar I.

Strain in the flanges was measured by Tuckerman strain gages J for specimens 7E, 7F, 8E, and 8F. The gages were attached near the center of specimens 7E and 7F and near the center of the shear bay of specimens 8E and 8F. The gages on specimens 8E and 8F were attached to measure the effect on the flange stresses of diagonal tension in the shear bays.

Results of transverse load tests.- The observed center deflection of specimens 7A to 7F is compared in figure 15 with that calculated from equation (2). The measured and calculated deflections agreed within 7 percent for flange stresses below 30,000 lb/in.^{2}. Above this stress yielding of the material caused the observed center deflection to exceed the calculated center deflection.

The observed center deflection of specimens 8A to 8F is compared in figure 16 with that calculated from equation (2). The observed and calculated deflections agreed within 9 percent for average shear stresses below about 3500 lb/in.^{2}. Above this stress, buckling of the web as well as yielding of the material caused the observed center deflection to increase more rapidly than the calculated center deflection.

The average extreme fiber stresses obtained from strain-gage readings near the center of specimens 7E and 7F are compared with the values computed from the simple beam theory in figure 17. The two values were in close agreement, the maximum deviation being less than 6 percent.

The extreme fiber stresses obtained from strain gages at the center of the shear bay in specimens 8E and 8F are compared with the values computed from the simple beam theory in figure 18. The stresses for specimen 8E agree within 10 percent up to an average shearing stress P_b/A of about

2700 lb/in.^{2} at which diagonal wrinkles became noticeable in the shear web. (See fig. 8e.) The divergence above this load may be explained as follows. The horizontal component of the diagonal tension in the shear wrinkle must be balanced by compressive forces acting on the flanges; these would lower the tensile stress in the tension flange and raise the compressive stress in the compression flange. The stresses for specimen 8F agree within 10 percent except for values of average shearing stress, P_b/A, below 1500 lb/in.^{2}. No shear wrinkles were observed in specimen 8F.

The conditions at failure of specimens under transverse load are given in tables 3A to 3E. Failure was due to instability of the flanges for specimens 7A to 7F and for specimen 8F. For specimen 8A, failure was due to buckling of the shear web; while for specimens 8B to 8E failure was preceded by severe diagonal tension wrinkles in the shear web. The tension developed by these wrinkles caused failure of rivets connecting web to flange in the case of specimens 8D and 8E, buckling of the compression flange in the case of specimen 8B, and rupture of the shear web through a rivet hole at a web stiffener in the case of beam 8C.

Beam 7C tipped suddenly when subjected to a bending moment of 55,300 pound-inches because the lower ends of several of the angle-iron type guides ceased to be effective when the specimen bent sufficiently to bring the lower flange below the guides. The short guides were replaced by longer guides and the test was continued. The beam finally failed at 57,580 lb-in. This is a low value for this type of beam, and it is probable that the sudden tipping in the first test caused premature failure upon reloading.

The shear loads at failure, the average shearing stress at failure, and the shearing stress obtained by dividing the load at failure P_b by the area ht of a rectangular section having the height of the beam section and the thickness of the web, are given in table 4 for specimens 8A to 8F. The average shear stress P_b/A ranged from 2420 lb/in.^{2} for specimen 8F to 9860 lb/in.^{2} for specimen 8A. The average stress P_b/ht ranged from 5230 lb/in.^{2} for specimen 8F to 36,480 lb/in.^{2} for specimen 8A.

ANALYSIS

Stiffness

The deflection of a beam at low loads may be computed from the simple beam theory if the load, the length dimensions, the moduli E, G, and the section constants A, I, and k, where k denotes the shear constant, are known. Comparison of calculated and observed deflections in figures 12a to 12f, 15, and 16 below stresses for which yielding was appreciable shows that the differences between observed and calculated deflections did not exceed 10 percent for most of the observed points. This indicates that the section constants, determined from the dimensions of the section without regard for web buckling, are adequate in determining deflection. Low observed deflections for specimens 5A, 4C, and 4D were attributed to excessive friction in the machine shown in figure 10.

A similar comparison of measured and computed extreme fiber strains or stresses (figs. 9B to 9F, 13B to 13F, 17, and 18) shows that the section constants determined from the dimensions of the sections are adequate in determining extreme fiber strain or stress at low loads.

By reversing the argument, measurements of extreme fiber strain at low loads may be used to determine the section constants A and I by substitution in the following equations taken from the simple beam theory:

$$\sigma_1 = -\frac{P_c}{A} - \frac{M_b h}{2I}$$

$$\sigma_2 = -\frac{P_c}{A} + \frac{M_b h}{2I} \qquad (4)$$

σ_1, σ_2 = extreme fiber stresses, positive when tensile h = height of section

Solving for A and I gives

$$A = -2\frac{1}{\sigma_1/P_c + \sigma_2/P_c}$$

$$I = -\frac{h}{\sigma_1/M_b - \sigma_2/M_b} \qquad (5)$$

These formulas were applied by using the measured strain together with the tensile and compressive stress-strain curves (figs. 2b to 2f) to determine σ_1 and σ_2 and by substituting for σ/P_c and σ/M_b values of the slope of a straight line faired through a plot of σ versus P_c and σ versus M_b at low loads. These values are compared in table 5 with the values of A and I computed from measured dimensions of the cross section. The averages of the measured values were from 5 percent less to 3 percent greater than the computed values. This indicates that the simple beam theory gives accurate values of extreme fiber stress at low loads for the beams included in the tests.

Dimensionless stiffness ratios for each type of beam were obtained by dividing the stiffness of each beam by the stiffness of a hypothetical beam having a weight per unit length equal to that of the specimen. For convenience it was assumed that the hypothetical beam had a rectangular section with depth equal to 12 times its width and that it consisted of aluminum alloy with a Young's modulus $E_o = 10.5 \times 10^6$ lb/in.^{2} and a density $\gamma_o = 0.1005$ pound per cubic inch. The dimensionless stiffness ratio is therefore

$$(EI)/(E_oI_o) = (EI)\Big/\left(\frac{E_o w^2}{\gamma_o^2}\right) = 9.62 \times 10^{-10}\,\frac{EI}{w^2}$$

Values of this dimensionless ratio are given in table 6 for purposes of comparing the effect of section shape and material on the stiffness. The weight w per unit length includes web stiffeners but excludes load fittings. The lowest stiffness ratio, 3.41, was found for the 24S-T I-beam D with curved flanges and thick web and the highest, 5.89, was found for the 24S-T I-beam C with parallel flanges and thin web.

Effect of Length on Loads at Failure for Column Specimens 1 and 2

The effect of length on the load at failure for the column specimens 1 and 2 is shown in figure 19. The abscissas and ordinates in this figure were taken from reference 9, they are defined as:

$$\lambda = \frac{l/r}{\pi\sqrt{E/F_{co}}}; \quad \sigma = \frac{f_c}{F_{co}}$$

where

r maximum principal radius of gyration of section

F_{co} compressive yield strength of flange material (offset = 0.2 percent), except for specimens 1A, 2A for which no yield strengths were measured, and for which F_{co} was taken as the average stress at failure for specimen 1A.

f_c average stress at failure

The open points in figure 19 represent values corrected for loss in strength due to premature failure by bending about the axis of least stiffness. The correction was made by estimating the load at which the extreme fiber stress in the beam would have reached a critical value for local buckling in the absence of bending about the axis of least stiffness. Approximate values of the critical stresses for local buckling were obtained by averaging the measured extreme fiber stress at failure given as f_{t_3} in tables 3C to 3E.

The points indicate an appreciable length effect for beams A, D, and E. The average stress at failure for beams B, C, and F was nearly independent of length. Specimens 1D and 1E were perhaps too long to give the short column strength, which may have been up to 10 percent greater than the corrected load at failure.

Strength Ratio

In order to compare the strengths on a nondimensional basis, strength ratios for the specimens were computed as the ratio of the strength to the strength of a hypothetical beam having the same weight per inch, w, as the specimen. It was again assumed for convenience that the hypothetical beam had a rectangular section with depth equal to 12 times its width. Furthermore, it was assumed that the beam would fail when the extreme fiber stress reached 40,000 lb/in.^{2} or when the shear stress reached 24,000 lb/in.^{2}. The density of the hypothetical beam was taken as 0.1005 lb/in.^{3}, which is characteristic of aluminum alloy. On this basis the axial

load at failure P_h for axial loading, the bending moment at failure M_h for flexural loading, and the shearing force at failure Q_h, for transverse shearing, is given by:

$$P_h = 398{,}000\ w \text{ (lb)}$$
$$M_h = 725{,}000\ w^{3/2} \text{ (lb-in.)} \qquad (6)$$
$$Q_h = 238{,}800\ w \text{ (lb)}$$

The strength ratios were computed by dividing the measured strengths of the specimen by the strength of the corresponding hypothetical beam. Corrected values for P_c and M_t, as indicated in parentheses in tables 3A to 3E, were used.

The strength ratios are listed in table 7. Type D has the highest strength ratio under axial load, type F has the highest strength ratio under bending load, and of types A to E, type D has the highest strength ratio under shear load. Type F should not be included in the shear load comparison since none of the beams of type F failed in shear.

The strength ratio under combined loads is shown in figure 20. Only those values in table 7 which were not marked as questionable are plotted. Type F has the highest strength ratio under combined axial and bending loads. The interaction curves for combinations of axial load and bending appear to be nearly straight lines within the scatter of measurements.

COMPUTATION OF STRENGTH UNDER COMBINED AXIAL AND TRANSVERSE LOADS FROM SHORT COLUMN STRENGTH AND FROM STRENGTH IN PURE BENDING

The interaction curves fitted to the observed strength ratios $\frac{P_c}{P_h}, \frac{M_t}{M_h}$ are shown in figure 20 to be straight lines. This fact may be applied as follows to compute the strength under combined load of wing beams similar to those tested.

Make a short column test of the wing beam to determine the short column strength P_{co}. A specimen with a slenderness ratio l/r of around 10 is probably adequate for this purpose. In some cases specimens of two or more lengths may have to be tested to ascertain that failure was free from column action.

Make a pure bending test to determine the bending moment at failure M_o.

The ratio of axial load at failure P_c and of total bending moment at failure M_t to P_{co} and M_o, respectively, is given by the interaction equation:

$$P_c/P_{co} + M_t/M_o = 1 \qquad (7)$$

The total bending moment

$$M_t = M_b + P_c\delta_c \qquad (8)$$

Osgood (reference 10) determines M_t for the case of round steel tubes by deriving an empirical relation between the observed value of the ratio of total bending moment to primary bending moment M_t/M_b and the value of $(M_t/M_b)_{calc}$ computed from the elastic beam theory. In order to derive a similar relation for wing beams, values of

$$\left(\frac{M_t}{M_b}\right)_{calc} = 1 + \frac{P_c(\delta_c)_{calc}}{M_b} \qquad (9)$$

were computed for each wing beam specimen from

P_c axial load at failure (lb)

M_b primary bending moment at failure (lb-in)

$(\delta_c)_{calc}$ center deflection from equation (2) (in.)

Values of the ratio M_t/M_b of the measured loads at failure, were obtained from equation (9) by replacing $(\delta_c)_{calc}$ by the experimental value of the center deflection at failure as given in tables 3A to 3E.

The values of M_t/M_b are plotted against $(M_t/M_b)_{calc}$ in figure 21. The points scatter about the straight line

$$M_t/M_b = 1.470\ (M_t/M_b)_{calc} - 0.470 \tag{10}$$

It must be remembered in using this straight line relationship that it represents an empirical method of taking account of the increased deflection due to yielding of the material. It does not necessarily apply to other sections than those tested or to beams of materials the stress-strain curves of which differ greatly from those of figures 2b to 2f. An example will be given to show how to compute P_c and M_b for a beam for which P_{co} and M_o are given. The method is a solution of equation 7 by trial and error.

Example:

Consider beam 6B for which the ratio of primary bending moment to axial load is fixed as

$$\frac{M_b}{P_c} = 5.50 \text{ in.} \tag{11}$$

and assume that a short-column test and a pure bending test of a beam of this type were made and that these tests gave

$$\begin{aligned} P_{co} &= 22{,}300 \text{ lb} \\ M_o &= 64{,}380 \text{ lb-in} \end{aligned} \tag{12}$$

These values correspond to the estimated loads for failure without lateral bending (table 3B). Values of $(\delta_c)_{calc}$ for three trial values of P_c (P_c = 6000, 6310, 6500 lb) were computed by substituting the known dimensions and section constants for beams of type B in equation (2). The results are plotted as curve A in figure 22.

The primary bending moments M_b corresponding to the trial values of P_c were computed from equation (11) and the ratios $(M_t/M_b)_{calc}$ from equation (9). These ratios are plotted as curve B. The values of M_t/M_b were derived

from equation (10). They are plotted as curve C in figure 22. The corresponding values of M_t/M_o are plotted as curve D and the values of P_c/P_{co} as curve E. Curve F shows the sum

$$\frac{P_c}{P_{co}} + \frac{M_t}{M_o} \tag{13}$$

The value of P_c corresponding to the interaction curve (equation (7)) is then given by the abscissa for which curve F is equal to unity. This gives

$$P_c = 6380 \text{ lb} \tag{14}$$

and from equation (11)

$$M_b = 5.5 \times 6380 = 35,100 \text{ lb-in} \tag{15}$$

The measured axial load and primary bending moment at failure were from table 3B:

$$P_c = 6310 \text{ lb}$$

$$M_b = 34,700 \text{ lb-in} \tag{16}$$

The values are in close agreement with the computed values.

The procedure illustrated in the example was applied to all wing beams tested under combined load in order to obtain an estimate of the errors.

The results based on corrected values of P_{co}, M_o are given in table 8. The maximum difference between observed and calculated loads at failure was equal to 14 percent.

National Bureau of Standards,
Washington, D. C., January 20, 1945.

REFERENCES

1. A.S.T.M. Standards 1939, Tension Testing of Metallic Materials, p. 756.

2. Aitchison, C. S., and Tuckerman, L. B.: The "Pack" Method for Compressive Tests of Thin Specimens of Materials Used in Thin-Wall Structures. NACA Rep. No. 649, 1939.

3. Marguerre, Karl: The Apparent Width of the Plate in Compression. NACA TM No. 833, 1937.

4. Levy, Samuel: Bending of Rectangular Plates with Large Deflections. NACA Rep. No. 737, 1942. (Issued also as TN No. 846, 1942.)

5. Levy, Samuel, and Krupen, Philip: Large-Deflection Theory for End Compression of Long Rectangular Plates Rigidly Clamped along Two Edges. NACA TN No. 884, 1943.

6. Timoshenko, S.: Theory of Elasticity. McGraw-Hill Book Co., Inc., New York, 1st ed., 1934.

7. Timoshenko, S.: Strength of Materials. D. Van Nostrand Co., Inc., New York, 1930.

8. Nölke, K.: Biegungsbeulung der Rechteckplatte. Ingenieur-Archiv, Bd. VIII, Heft 6, Dec. 1937, pp. 403-425.

9. Tuckerman, L. B., Petrenko, S. N., and Johnson, C. D.: Strength of Tubing under Combined Axial and Transverse Loading. NACA TN No. 307, 1929.

10. Osgood, William R.: Round Heat-Treated Chromium-Molybdenum-Steel Tubing under Combined Loads. NACA TN No. 896, 1943.

Table 1A
Dimensional Properties
Beams A

Specimen No.	$n = \frac{f_b}{f_t}$ [1]	length	Weight per unit length	A [3]	I_{max} [2]	ℓ/r [4]
		in.	lb/in.	in^2	in^4	
1A	0	22	.1142	0.364	1.85	4.89
2A	0	72	----	.370[x]	1.84[x]	32.3
3A	0.334	72	----	.370[x]	1.84[x]	32.3
4A	.185	120	----	.370[x]	1.84[x]	53.8
5A	.668	72	----	.370[x]	1.84[x]	32.3
6A	.668	120	----	.370[x]	1.84[x]	53.8
6A(Dupl.)	.664	120	----	.370[x]	1.84[x]	53.8
7A	1.000	72	.1268+	----	1.87[xx]	----
8A	1.000	46	.1337+	----	1.87[xx]	----

1 $n = \frac{f_b}{f_t} = \frac{\text{extreme fiber bending stress}}{\text{total extreme fiber stress}}$, at low loads

2 I_{max} = maximum principal moment of inertia of section

3 A = cross-sectional area

4 ℓ/r = slenderness ratio = $\ell\sqrt{A/I_{max}}$

\+ including fittings
x from nominal dimensions of section
xx from load-deflection curve of beam 7A.

Table 1B
Dimensional Properties
Beams B

Specimen No.	$n = \frac{f_b}{f_t}$ [1]	length	Weight per unit length	A [3]	I_{max} [2]	ℓ/r [4]
		in.	lb/in	in^2	in^4	
1B	0	29.7	.1000	----	----	11.2
2B	0	72.0	.0988	----	----	27.2
3B	0.369	72.0	.1115+	0.819	5.70	27.2
4B	.347	120.0	.1048+	.792	5.45	45.3
5B	.698	72.0	.1114+	.812	5.63	27.2
6B	.705	120.0	.1049+	.799	5.55	45.3
7B	1.000	72.0	.1214+	----	----	----
8B	1.000	48.6	.1302+	----	----	----

1 $n = \frac{f_b}{f_t} = \frac{\text{extreme fiber bending stress}}{\text{total extreme fiber stress}}$, at low loads

2 I_{max} = maximum principal moment of inertia of section

3 A = cross-sectional area

4 ℓ/r = slenderness ratio = $\ell\sqrt{A/I_{max}}$, where the values A = 0.802 in^2 and I = 5.63 in^4 were used for all the specimens. A = 0.802 in^2 is practically equal to the average of the measured areas; I_{max} = 5.63 in^4 is about 1 percent higher than the average of the measured values and was derived as that value of I which gave the best fit to the observed load-deflection curve for specimens 7B and 8B.

\+ including fittings

Table 1C
Dimensional Properties
Beams C

Specimen No.	$n = \frac{f_b}{f_t}$ [1]	length	weight per unit length	A [3]	I_{max} [2]	ℓ/r [4]
		in.	lb/in.	in^2	in^4	
1C	0	29.7	0.0964	----	----	11.2
2C	0	72.0	.0977	----	----	27.2
3C	0.373	72.0	----	.810	5.60	27.2
4C	.347	120.0	.1048+	.814	5.58	45.3
5C	.699	72.0	.1109+	.795	5.49	27.2
6C	.705	120.0	.1019+	.782	5.37	45.3
7C	1.000	72.0	.1192+	----	----	----
8C	1.000	48.6	.1274	----	----	----

1 $n = \frac{f_b}{f_t} = \frac{\text{extreme fiber bending stress}}{\text{total extreme fiber stress}}$, at low loads

2 I_{max} = maximum principal moment of inertia of section

3 A = cross-sectional area

4 ℓ/r = slenderness ratio $= \ell\sqrt{A/I_{max}}$, where the values A = 0.802 in^2 and I_{max} = 5.63 in^4 were used for all specimens. A = 0.802 in^2 is practically equal to the average of the measured areas, I_{max} = 5.63 in^4 is about 2 percent higher then the average of the measured values and was derived as that value of I which gave the best fit to the observed load deflection curve for specimens 7C and 8C.

+including fittings

Table 1D
Dimensional Properties
Beams D

Specimen No.	$n = \frac{f_b}{f_t}$ [1]	length	weight per unit length+	A [3]	I_{max} [2]	ℓ/r [4]
		in.	lb/in.	in^2	in^4	
1D	0	29.8	0.106	----	----	17.1
2D	0	65.8	.106	----	----	37.8
3D	0.358	41.0	.126	0.885	2.70	23.6
4D	.335	54.0	.109	.873	2.63	31.0
5D	.691	41.0	.125	.896	2.71	23.6
6D	.691	54.0	.109	.869	2.66	31.0
7D	1.000	54.0	.130	----	----	----
8D	1.000	18.0	.193	----	----	----

1 $n = \frac{f_b}{f_t} = \frac{\text{extreme fiber bending stress}}{\text{total extreme fiber stress}}$, at low loads

2 I_{max} = maximum principal moment of inertia of section

3 A = cross-sectional area

4 ℓ/r = slenderness ratio $= \ell\sqrt{A/I_{max}}$, where the average values A = 0.881 in^2 and I_{max} = 2.68 in^4 were used for all the beams.

+including fittings

Table 1E
Dimensional Properties
Beams E

Specimen No.	$n = \frac{f_b}{f_t}$ [1]	length	Weight per unit length	A [3]	I_{max} [2]	ℓ/r [4]
		in.	lb/in.	in^2	in^4	
1E	0	41.2	0.0852	0.824	3.81	19.2
2E	0	77.2	.0841	.830	3.83	35.9
3E	0.329	77.2	.0918+	----	----	35.9
4E	.329	86.2	.0898+	----	----	40.1
5E	.663	77.2	.0927+	----	----	35.9
6E	.663	86.2	.0893+	----	----	40.1
7E	1.000	72.0	.1290+	----	----	----
8E	1.000	36.0	.1674+	----	----	----

1 $n = \frac{f_b}{f_t} = \frac{\text{extreme fiber bending stress}}{\text{total extreme fiber stress}}$, at low loads

2 I_{max} = maximum principal moment of inertia of section

3 A = cross-sectional area

4 ℓ/r = slenderness ratio = $\ell\sqrt{A/I_{max}}$, where the average values A = 0.827 in^2 and I_{max} = 3.82 in^4 were used for all the beams.

+including fittings

Table 1F
Dimensional Properties
Beams F

Specimen No.	$n = \frac{f_b}{f_t}$ [1]	length	Weight per unit length	A [3]	I_{max} [2]	ℓ/r [4]
		in.	lb/in.	in^2	in^4	
1F	0	8.30	----	0.777	----	5.1
2F	0	58.2	0.0507	.776	2.06	28.0
3F	0.342	58.2	.0508	.778	2.05	35.7
4F	.342	83.4	.0509	.780	----	51.2
5F	.675	58.2	.0505	.774	2.06	35.7
6F	.675	83.4	.0509	.779	2.06	51.2
7F	1.000	57.9	----	----	----	----
8F	1.000	22.5	----	----	----	----

1 $n = \frac{f_b}{f_t} = \frac{\text{extreme fiber bending stress}}{\text{total extreme fiber stress}}$, at low loads

2 I_{max} = maximum principal moment of inertia of section

3 A = cross-sectional area

4 ℓ/r = slenderness ratio = $\ell\sqrt{A/I_{max}}$, where the average values A = 0.777 in^2 and I_{max} = 2.06 in^4 were used for all the beams.

Table 2

Mechanical Properties of Beam Material
(Average values)

Specimen	Young's modulus		Yield strength*		Tensile strength	Elongation in 2 in.
	tension	compression	tension	compression		
	$lb/in^2 \times 10^6$	$lb/in^2 \times 10^6$	lb/in^2	lb/in^2	lb/in^2	per cent
1A	----	27.3	------	------	------	----
B. flanges	10.2	10.7	39,000	35,800	57,600	25.0
B. web	10.4	----	36,300	------	59,000	19.2
C. flanges	10.1	10.6	50,800	44,600	67,500	19.7
C. web	10.4	----	58,300	------	68,000	16.0
D. flanges	10.3	10.4	46,800	42,400	59,000	19.2
E. flanges	10.4	10.5	44,300	37,000	62,800	20.1
E. web	10.4	----	38,600	------	59,000	18.3
F. flanges	6.4	6.7	33,000	33,200	52,600	9.0

*offset = 0.2 per cent

Table 3A. Loads, deflections, and stresses at failure, beams A

Specimen	type	slenderness ratio l/r[a]	initial ratio $n=f_b/f_t$	P_c	M_b	δ_c	f_{t1}	f_{t2}	f_{t3}	Type of failure
				lb	lb-in.	in.	lb/in^2	lb/in^2	lb/in^2	
1A	short column	4.89	0	30,700	-	-	84,400	-	-	Crinkling of flanges and web
2A	long column	32.3	0	25,200[c]	-	-	68,200	-	-	Crinkling of flanges and web
3A	combined	32.3	.334	20,000	16,400	.500[b]	90,600	98,700[b]	-	Crinkling of flanges and web
4A	combined	53.8	.185	19,600	7,140	1.060[b]	81,600	99,400	-	Crinkling of flanges and web
5A	combined	32.3	.668	11,900	39,100	.760[b]	108,100	112,200	-	Crinkling of flanges and web
6A	combined	53.8	.660	8,740	27,700	2.280	85,500	102,800	-	Crinkling of flanges and web
6A dupl.	combined	53.8	.664	9,280	29,200	2.020	97,400	108,900	-	Crinkling of flanges and web
7A	transverse bend	----	1.000	-	58,700 (67,500)[d]	.83[b]	95,800	95,800	-	Crinkling of compression flange near load point
8A	transverse shear	----	1.000	-	29,200	.19[b]	54,200[b]	54,200	-	Crinkling of web in shear portion

[a]value for bending about axis of maximum stiffness
[b]extrapolated value
[c]strain gages indicate bending about axis of least stiffness
P_c = axial load
M_b = bending moment
δ_c = center deflection
f_{t1} = total extreme fiber stress, from measured loads and calculated deflection, at failure
f_{t2} = " " " " , " " " " measured " , " "
f_{t3} = " " " " , " strain gages
[d] = estimated load at failure without stress concentration at intermediate load points

Table 3B. Loads, deflections, and stresses at failure, beams B

Specimen	Type	slenderness ratio ℓ/r[a]	initial ratio $n=f_b/f_t$	P_o	M_b	δ_o	f_{t1}	f_{t2}	f_{t3}	Type of failure
				lb	lb-in.	in.	lb/in^2	lb/in^2	lb/in^2	
1B	short column	11.2	0	22,720[c] (22,300)	-	-	28,300	-	31,500[b]	Buckling of flange near middle
2B	long column	27.2	0	21,600	-	-	26,900	-	34,600[b]	Buckling of flange near middle
3B	combined	27.2	.369	13,000	17,500	.262	27,300	27,600	32,200	Buckling of flange near middle
4B	combined	45.3	.347	13,110	16,000	.906	29,800	31,400	31,800	Buckling of flange off-center
5B	combined	27.2	.698	6,350	33,600	.425	27,500	27,600	31,500	Buckling of flange near middle
6B	combined	45.3	.705	6,310	34,700	1.417	30,600	31,500	32,200	Buckling of flange off-center
7B	transverse bend	-	1.000	-	64,400	.811	34,900	34,900	-	Buckling of compression flange
8B	transverse shear	-	1.000	-	51,000	.510	27,600[b]	27,600	-	Buckling of compression flange near end

[a]value for bending about axis of maximum stiffness
[b]extrapolated value
[c]strain gages indicate either bending about axis of least stiffness or rotation of flanges toward each other
Value in parentheses is load at failure without lateral bending, estimated from combined load tests
P_o = axial load
M_b = bending moment
δ_o = center deflection
f_{t1} = total extreme fiber stress, from measured loads and calculated deflection, at failure
f_{t2} = " " " " , " " " " measured " , " "
f_{t3} = " " " " , " strain gages

Table 3C. Loads, deflections, and stresses at failure, beams C

Specimen	Type	slenderness ratio ℓ/r[a]	initial ratio $n=f_b/f_t$	P_o	M_b	δ_o	f_{t1}	f_{t2}	f_{t3}	Type of failure
				lb	lb-in.	in.	lb/in^2	lb/in^2	lb/in^2	
1C	short column	11.2	0	24,900[c] (27,400)	-	-	31,100	-	35,000[b]	Buckling of flange
2C	long column	27.2	0	27,400	-	-	34,200	-	38,600[b]	Buckling of flange
3C	combined	27.2	.373	15,300	20,800	.296	32,500	32,600	38,600	Buckling of flange off-center
4C	combined	45.3	.347	14,100[e]	17,200[e]	.791[e]	34,200[e]	34,200[e]	-	Buckling of flange off-center
5C	combined	27.2	.699	7,440	39,700	.477	32,600	33,200	37,700	Buckling of flange near middle
6C	combined	45.3	.705	7,130	39,200	1.394	35,300	35,600	40,500	Buckling of flange
7C	transverse bend	-	1.000	-	57,600 (70,500)[f]	.655	31,200	31,200 (36,200)	-	Buckling of flange after lateral instability in previous test
8C	transverse shear	-	1.000	-	60,800	.618	32,900[b]	32,900	-	Tearing of web in shear portion

[a]value for bending about axis of maximum stiffness
[b]extrapolated value
[c]strain gages indicate either bending about axis of least stiffness or rotation of flanges toward each other. Value in parentheses is load at failure without lateral bending, estimated from combined load tests.
[e]results doubtful, due to excessive friction in testing machine
[f]estimated load at failure without lateral instability in previous test.
P_o = axial load
M_b = bending moment
δ_o = center deflection
f_{t1} = total extreme fiber stress, from measured loads and calculated deflection, at failure
f_{t2} = " " " " , " " " " measured " , " "
f_{t3} = " " " " , " strain gages

Table 3D. Loads, deflections, and stresses at failure, beams D

Specimen	Type	slenderness ratio l/r[a]	initial ratio $n=f_b/f_t$	P_c	M_b	δ_c	f_{t1}	f_{t2}	f_{t3}[d]	Type of failure
				lb	lb-in.	in.	lb/in^2	lb/in^2	lb/in^2	
1D	short column	17.1	0	27,800[c] (33,200)	-	-	31,500	-	35,600	Buckling of flange
2D	long column	37.8	0	25,800[c] (29,600)	-	-	29,300	-	31,500	Buckling of flange
3D	combined	23.6	.358	20,500	16,400	.198	38,400	39,500	41,900	Buckling of flange near middle
4D	combined	31.0	.335	18,400[e]	13,400[e]	.187[eb]	34,400[e]	34,100[eb]	37,200[eb]	Buckling of flange off-center
5D	combined	23.6	.691	11,000	35,100	.334	42,700	43,300	41,500	Buckling of flange near middle
6D	combined	31.0	.691	9,340	29,800	.488[b]	37,400	37,900[b]	38,200[b]	Buckling of flange off-center
7D	transverse bend	-	1.000	-	64,100	.87[b]	50,900	50,900	-	Buckling of flange
8D	transverse shear	-	1.000	-	44,600	-	35,200	35,200	-	Shearing of rivets in shear portion

[a]value for bending about axis of maximum stiffness
[b]extrapolated value
[c]strain gages indicate either bending about axis of least stiffness or rotation of flanges toward each other. Value in parentheses is load at failure without lateral bending, estimated from combined load tests.
[d]average compressive stress on gages
[e]results doubtful, due to excessive friction in testing machine
P_c = axial load
M_b = bending moment
δ_c = center deflection
f_{t1}= total extreme fiber stress, from measured loads and calculated deflection, at failure
f_{t2}= " " " " , " " " " measured " , " "
f_{t3}= " " " " , " strain gages

Table 3E. Loads, deflections, and stresses at failure, beams E

Specimen	Type	slenderness ratio l/r[a]	initial ratio $n=f_b/f_t$	P_c	M_b	δ_c	f_{t1}	f_{t2}	f_{t3}[d]	Type of failure
				lb	lb-in	in.	lb/in^2	lb/in^2	lb/in^2	
1E	short column	19.2	0	25,000[c] (27,000)	-	-	30,200	-	38,700[b]	Buckling of flange
2E	long column	35.9	0	21,600[c] (25,200)	-	-	26,000	-	38,500	Buckling of flange
3E	combined	35.9	.329	16,300	14,800	.59	33,000	35,700	37,100	Buckling of flange at middle
4E	combined	40.1	.329	14,700	13,300	.80	30,300	34,300	38,000	Buckling of flange at middle
5E	combined	35.9	.663	8,640	31,400	.87[b]	34,700	36,000[b]	37,500[b]	Buckling of flange at middle
6E	combined	40.1	.663	8,320	30,200	1.08[b]	34,300	35,800[b]	38,600[b]	Buckling of flange at middle
7E	transverse bend	-	1.000	-	58,200	1.25[b]	38,200	38,200	38,000[b]	Buckling of flange
8E	transverse shear	-	1.000	-	47,050	.53[b]	30,900	30,900	-	Shearing of rivets in shear portion

[a]value for bending about axis of maximum stiffness
[b]extrapolated value
[c]strain gages indicate either bending about axis of least stiffness or rotation of flanges towards each other. Value in parentheses is load at failure without lateral bending, estimated from combined load tests.
[d]from maximum compressive strain read on any gage
P_c = axial load
M_b = bending moment
δ_c = center deflection
f_{t1}= total extreme fiber stress, from measured loads and calculated deflection, at failure
f_{t2}= " " " " , " " " " measured " , " "
f_{t3}= " " " " , " strain gages

Table 3F. Loads, deflections, and stresses at failure, beams F

Specimen	Type	slenderness ratio ℓ/r^a	initial ratio $n=f_b/f_t$	P_c	M_b	δ_c	f_{t1}	f_{t2}	f_{t3}^d	Type of failure
				lb	lb-in.	in.	lb/in^2	lb/in^2	lb/in^2	
1F	short column	5.1	0	16,500	-	-	21,300	-	26,800[b]	Buckling of flange
2F	long column	28.0	0	15,800	-	-	20,300	-	22,400[b]	Buckling of flange
3F	combin i	35.7	.342	11,500	7,940	0.39[b]	26,200	26,800[b]	28,000[b]	Buckling of flange
4F	combined	51.2	.342	10,300	7,150	.95[b]	29,700	29,700[b]	30,000[b]	Buckling of flange
5F	combined	35.7	.675	6,950	19,200	.75[b]	32,400	32,600[b]	32,000[b]	Buckling of flange
6F	combined	51.2	.675	6,000	16,600	1.52[b]	32,500	32,600[b]	33,000[b]	Buckling of flange
7F	transverse bend	-	1.000	-	36,300	1.15[b]	35,500	35,500	-	Buckling of flange
8F	transverse shear	-	1.000	-	37,200	.20	36,300	36,300	-	Buckling of flange

[a] value for bending about axis of maximum stiffness; ℓ = half length for flat end column tests
[b] extrapolated value
[d] from strain at center of flange
P_c = axial load
M_b = bending moment
δ_c = center deflection
f_{t1} = total extreme fiber stress, from measured loads and calculated deflection, at failure
f_{t2} = " " " " , " " " " measured " , " "
f_{t3} = " " " " , strain gages

Table 4

Shear Specimens at Failure

No.	Area* A	Web[x] h	Web[x] t	Shear load P_b	Shear Stress $\frac{P_b}{A}$	Shear Stress $\frac{P_b}{ht}$	Type of failure
	in^2	in.	in.	lb	lb/in^2		
8A	0.370	5.00	0.020	3650	9860	36500	buckling of shear web
8B	0.802	6.1	0.0325	5480	6830	27600	buckling of compression flange in shear bay
8C	0.802	6.1	0.0325	6520	8140	33000	rupture of shear web
8D	0.881	4.25	0.063	7420	8430	27800	failure of rivets in shear web
8E	0.827	5.00	0.0417	3920	4740	18800	" "
8F	0.777	4.00	0.090	1880**	2420**	5230**	failure in bending

[x] h = height of section in plane of web
t = thickness of web

* Estimated from measured values, table 1A to 1F

** Failed in bending. For failure in shear, this value might be larger.

Table 5

Calculated and Measured Section Constants

Beam	From sectional dimensions A	From sectional dimensions I	From stress-load curve at low loads A	From stress-load curve at low loads I
	in^2	in^4	in^2	in^4
1 A	0.364	1.846	---	---
2 A	-----	-----	---	---
3 A	-----	-----	---	---
4 A	-----	-----	---	---
5 A	-----	-----	---	---
6 A	-----	-----	---	---
7 A	-----	-----	---	---
8 A	-----	-----	---	---
Avg.	.364	1.846	---	---
1 B	-----	-----	0.809	----
2 B	-----	-----	.811	----
3 B	0.819	5.70	.865	5.61
4 B	.792	5,45	.827	5.40
5 B	.812	5.63	.847	5.43
6 B	.799	5.55	.808	5.27
7 B	-----	----	----	----
8 B	-----	----	----	----
Avg.	0.805	5.58	0.828	5,43
1 C	-----	----	0.756	----
2 C	-----	----	.794	----
3 C	0.810	5.60	.750	5.33
4 C	.814	5.58	-----	----
5 C	.795	5.49	.790	5.45
6 C	.782	5.37	.818	5.48
7 C	-----	----	-----	----
8 C	-----	----	-----	----
Avg.	0.800	5.51	0.780	5.42
1 D	-----	----	0.870	----
2 D	-----	----	.872	----
3 D	0.885	2.70	.882	2.41
4 D	.873	2.63	-----	----
5 D	.896	2.71	.953	2.74
6 D	.869	2.66	.878	2.53
7 D	-----	----	-----	----
8 D	-----	----	-----	----
Avg.	0.881	2.68	0.871	2.56
1 E	0.824	3.81	0.840	----
2 E	.830	3.83	.830	----
3 E	-----	----	.825	3.67
4 E	-----	----	.808	3.85
5 E	-----	----	.827	3.81
6 E	-----	----	.823	3.91
7 E	-----	----	----	3.72
8 E	-----	----	----	3.57
Avg.	0.827	3.82	0.825	3.75
1 F	0.777	----	----	----
2 F	.776	2.06	----	----
3 F	.778	2.05	0.777	2.11
4 F	.780	----	.750	2.13
5 F	.774	2.06	.724	2.08
6 F	.779	2.06	.764	2.09
7 F	-----	----	----	2.15
8 F	-----	----	----	2.09
Avg.	0.777	2.06	0.754	2.11

Table 6

Stiffness Ratio

Type	Description	Flexural rigidity EI lb-in^2	Weight per unit length w lb/in[x]	Dimensionless stiffness ratio $(EI)/(\frac{E_o w^2}{\gamma_o^2})$[xx]
A	stainless steel box beam	5.02×10^7	0.1142	3.70
B	17S-T Al I beam parallel flanges	5.74×10^7	0.0994	5.59
C	24S-T Al I beam parallel flanges	5.74×10^7	0.0968	5.89
D	24S-T Al I beam curved flanges	2.76×10^7	0.0883	3.41
E	17S-T Al I beam tilting flanges	3.98×10^7	0.0840	5.42
F	AM59S-T Mg I beam parallel flanges	1.35×10^7	0.0510	5.00

[x] not including weight of fittings

[xx] $\frac{E_o w^2}{\gamma_o^2}$ = stiffness of hypothetical rectangular beam of depth 12 times its width, having a weight per unit length equal to that of the beam and made of aluminum alloy having $E_o = 10.5 \times 10^6$ lb/in^2 and $\gamma_o = 0.1005$ lb/in^3.

Table 7 - Strength ratios

Weight w, lb/in [a]

Type	A	B	C	D	E	F
Beams 1 to 8	0.1142	0.0994	0.0968	0.0883	0.0840	0.0510

Axial load ratio, P_c/P_h [a]

Type	A	B	C	D	E	F
1	0.676	0.563	0.713[d]	0.944[d]	0.808[d]	0.814
2	.556[d]	.544	.714	.844[d]	.754[d]	.778
3	.445	.329	.398	.583	.488	.566
4	.432	.331	.366[d]	.524[d]	.440	.509
5	.262	.160	.193	.312	.258	.342
6	.198[c,d]	.159	.185	.264	.249	.296

Total bending moment ratio, M_t/M_h [a]

Type	A	B	C	D	E	F
3	0.948	.922	1.161	1.078	1.380	1.487
4	0.998	1.227	1.298[d]	.878[d]	1.420	2.030
5	1.720	1.600	1.981	2.061	2.207	2.951
6	1.709[c,d]	1.919	2.251	1.819	2.220	3.108
7	2.411[d]	2.835	3.230[d]	3.370	3.298	4.352
8	1.041	2.247	2.780	2.342	2.667	4.458

Shear load ratio, P_b/Q_h [a]

Type	A	B	C	D	E	F
8	0.134	0.231	0.283	0.352	0.196	0.155[b]

Table 7 - (continued)

[a]definition of symbols

w = weight per unit length of beam excluding fittings
P_c = axial load at failure
P_h = axial load at failure of hypothetical beam, equation 6
$M_t = M_b + P_c\delta_c$ = total bending moment at failure
M_h = total bending moment at failure for hypothetical beam, equation 6
P_b = shear load at failure
Q_h = shear load at failure for hypothetical beam, equation 6

[b]this beam failed in bending rather than shear. The shear load given is the shear load at failure in bending. A beam of the same type designed to fail in shear might fail at a higher shear load

[c]average for specimens 6A and 6A (dupl.)

[d]questionable value, see table 3

Table 8 - Comparison between measured loads and computed loads as outlined in section 5 for specimens under combined load.

Specimen	Measured loads		Computed loads		Difference
	Axial load P_c	Primary bending moment M_b	Axial load P_c	Primary bending moment M_b	
	lb	in-lb	lb	in-lb	percent
3A	20,200	16,500	19,900	16,200	+2
4A	19,600	7,140	19,700	7,180	-1
5A	11,900	39,100	10,900	35,800	+9
6A	8,740	27,700	9,210	29,200	-5
6A approx.	9,280	29,200	9,250	29,100	0
3B	13,000	17,500	14,000	18,800	-7
4B	13,100	16,000	12,800	15,600	+2
5B	6,350	33,600	7,280	38,500	-13
6B	6,310	34,700	6,400	35,200	- 1
3C	15,300	20,800	16,200	22,000	-6
4C	14,100	17,200	14,300	17,500	-2
5C	7,440	39,700	8,100	43,200	-8
6C	7,130	39,200	7,080	38,900	+1
3D	20,500	16,400	21,700	17,400	-6
4D	18,400	13,400	21,000	15,300	-12
5D	11,000	35,100	11,500	36,700	- 4
6D	9,340	29,800	10,900	34,800	-14
3E	16,300	14,700	16,300	14,700	0
4E	14,700	13,300	15,700	14,200	-6
5E	8,640	31,400	8,650	31,400	0
6E	8,320	30,200	8,450	30,700	-2
3F	11,500	7,940	11,100	7,660	+4
4F	10,300	7,150	9,340	6,460	+11
5F	6,950	19,200	6,400	17,700	+ 9
6F	6,000	16,600	5,510	15,200	+ 9

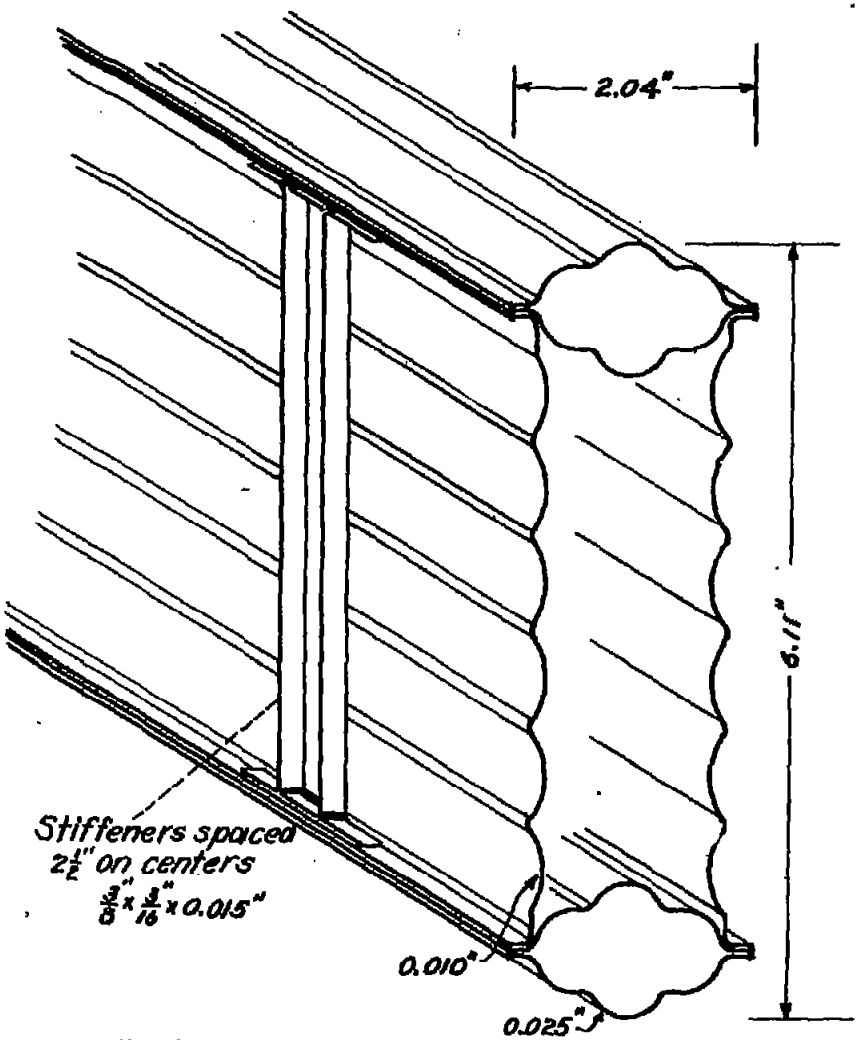

Fig. 1a.-
Type A - Stainless steel
box beam.

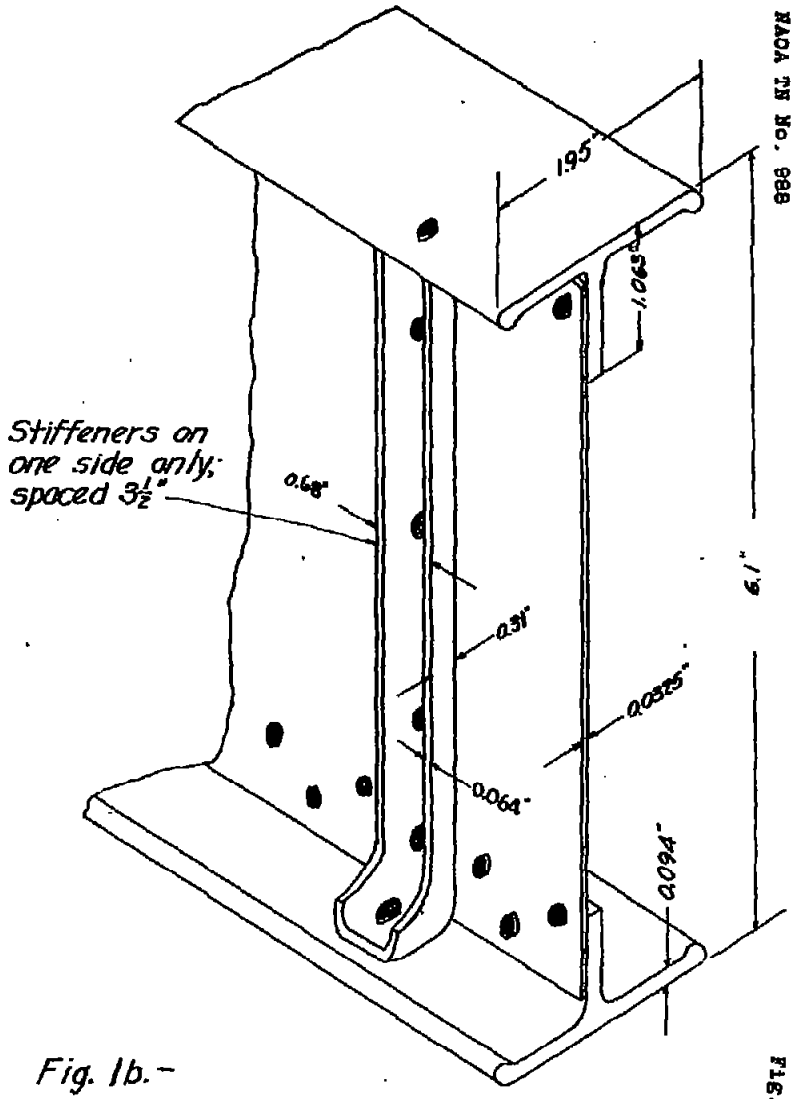

Fig. 1b.-
Type B. 17S-T aluminum alloy
I beam, straight flanges.

NACA TN No. 888

Fig. 1a,b

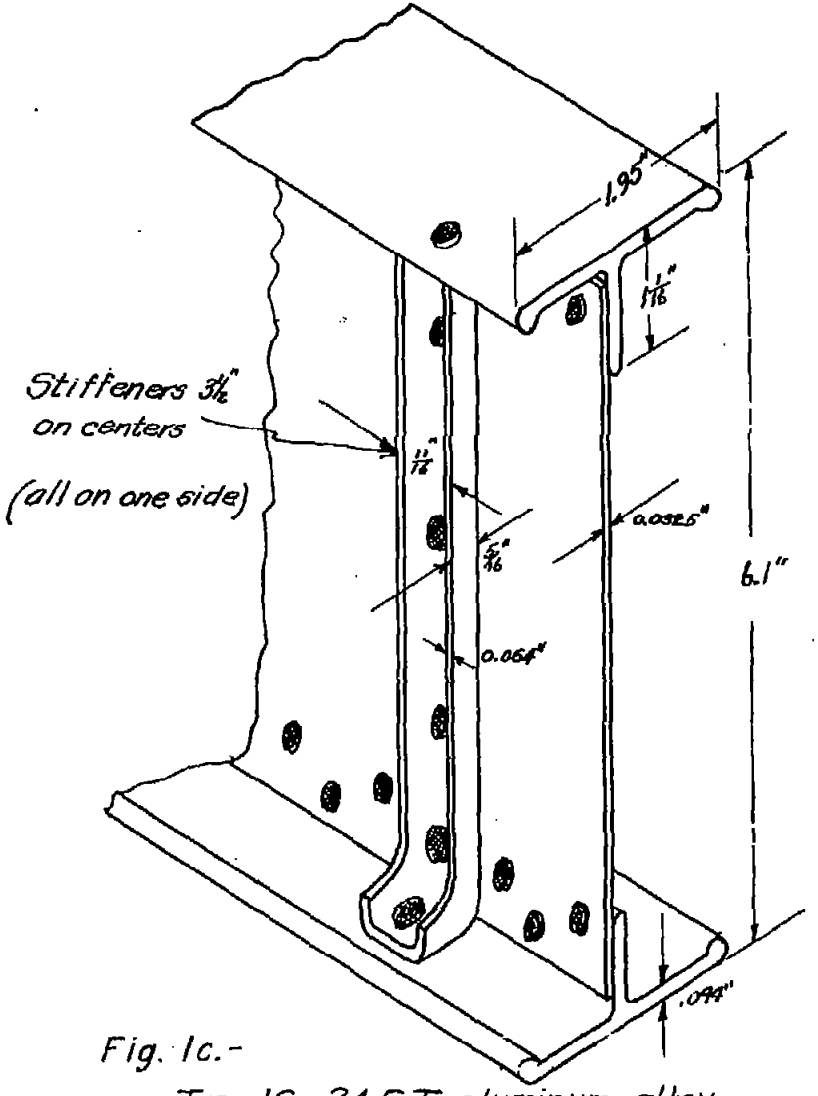

Fig. 1c.- Type 1C, 24 S-T aluminum alloy I beam, straight flanges.

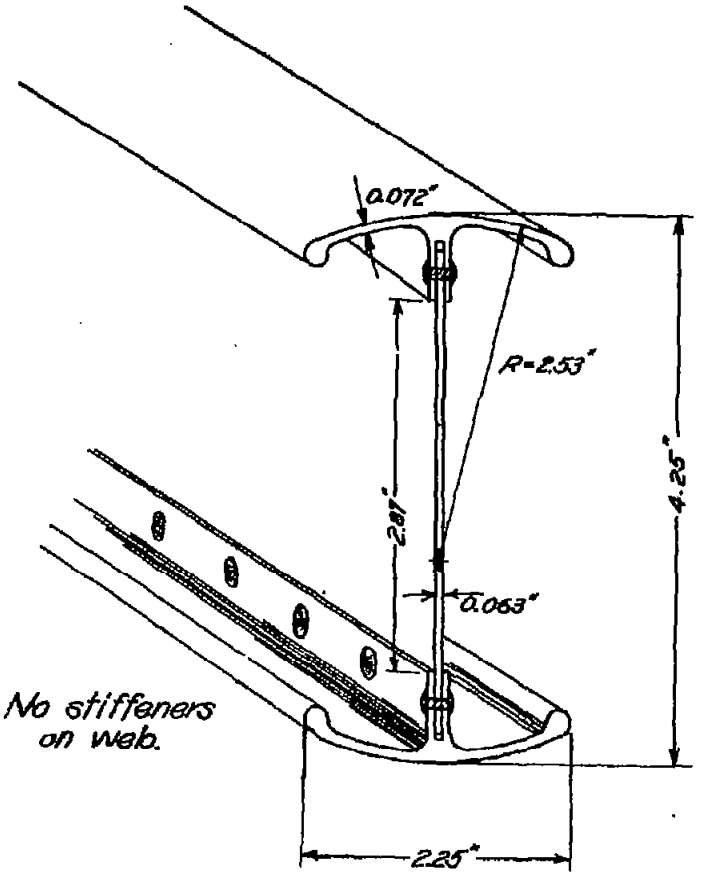

Fig. 1d.- Type 1D, 24 S-T aluminum alloy I beam, curved flanges.

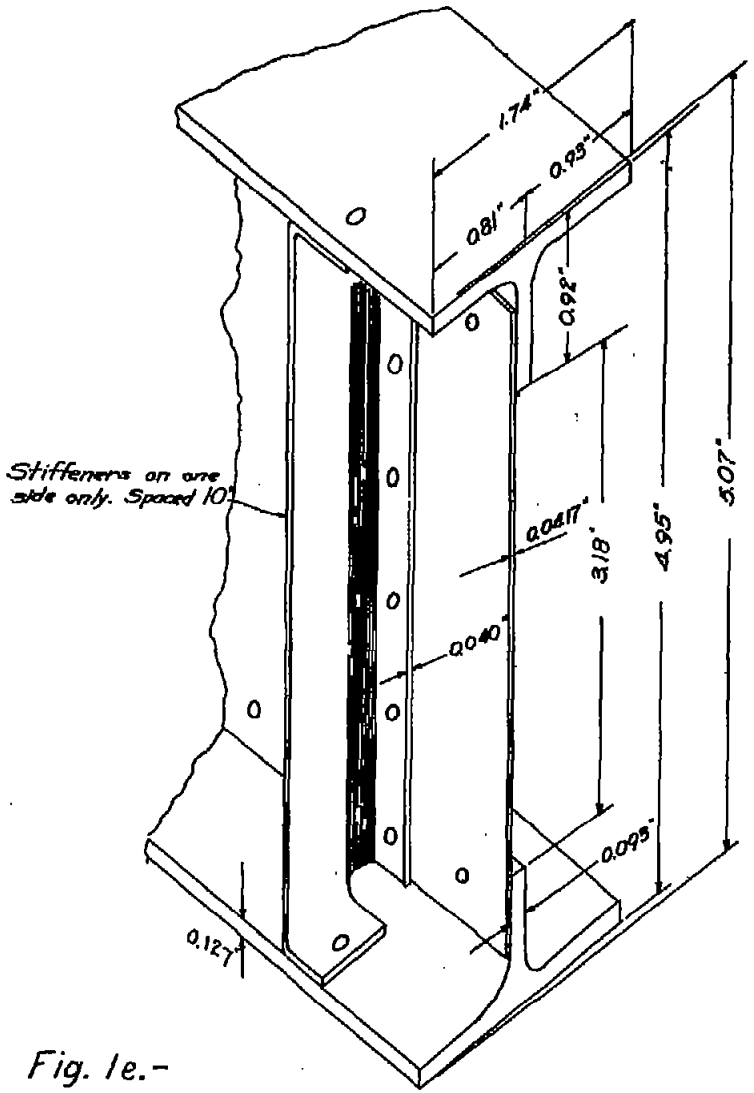

Fig. 1e.- Type E, 17S-T Aluminum alloy I beam, tilted flanges.

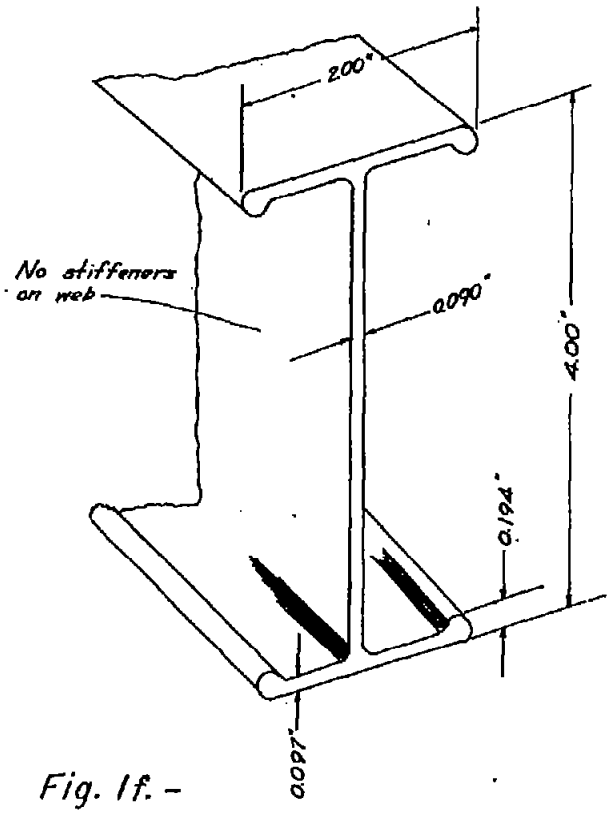

Fig. 1f.- Type F, AM 59S-T magnesium alloy I beam, straight flanges.

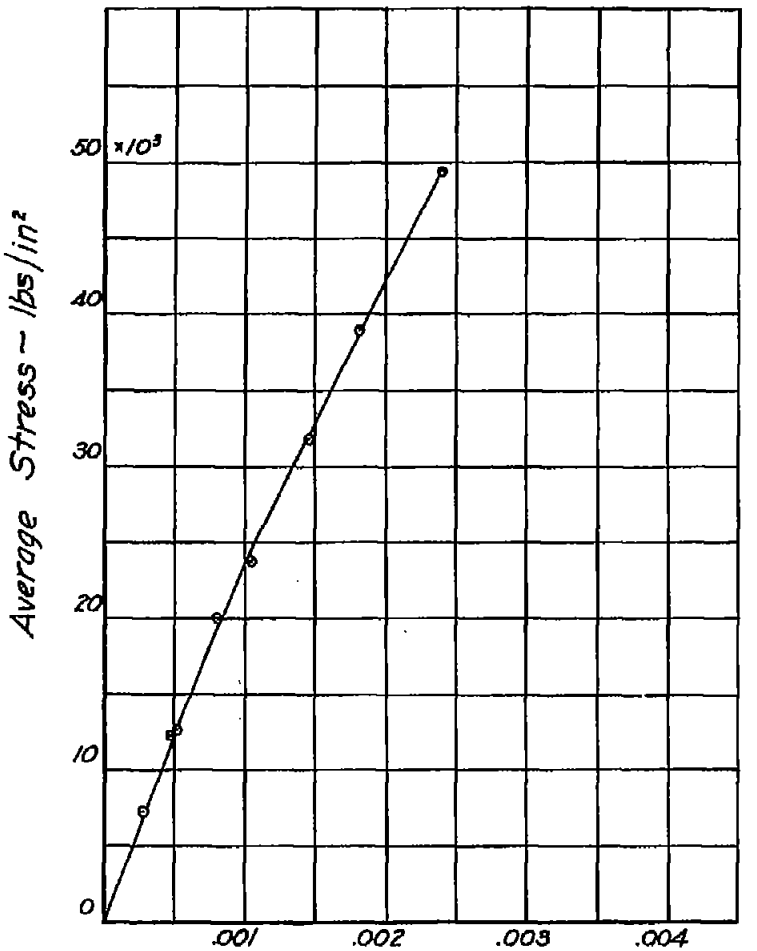

Fig. 2a.- Compressive stress-strain curve derived from test of short column 1A

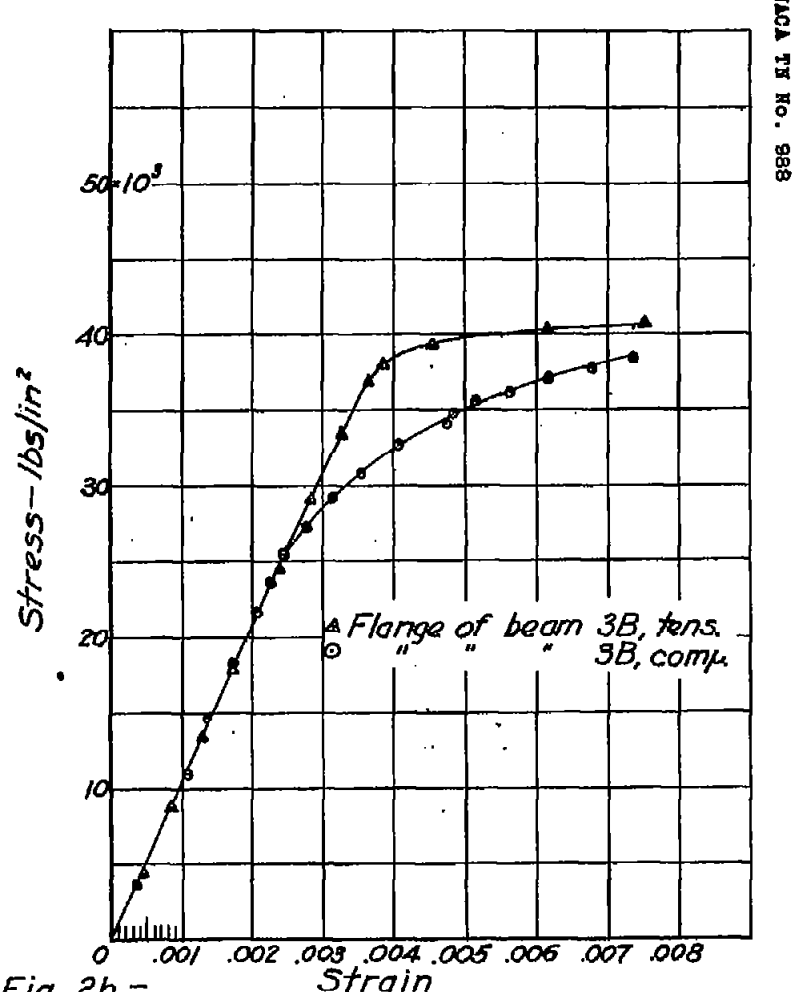

Fig. 2b.- Tensile and compressive stress-strain curves, flange material, beams B

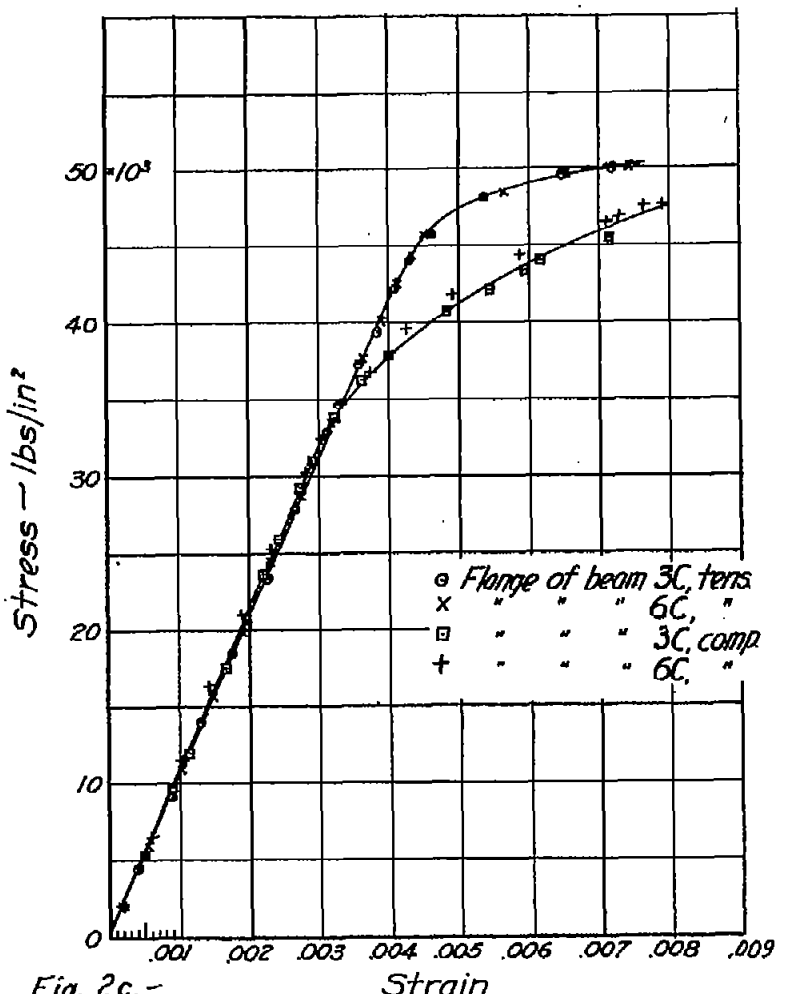

Fig. 2c. – Tensile and compressive stress-strain curve, flange material, beams C.

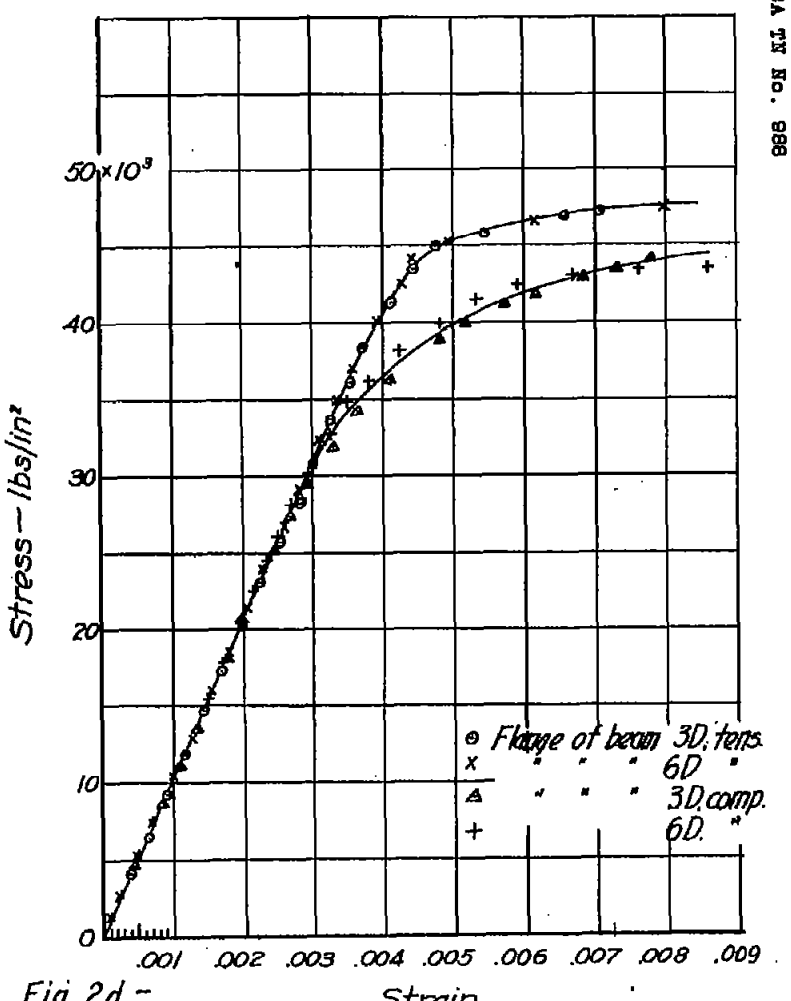

Fig. 2d. – Tensile and compressive stress-strain curve, flange material, beams D.

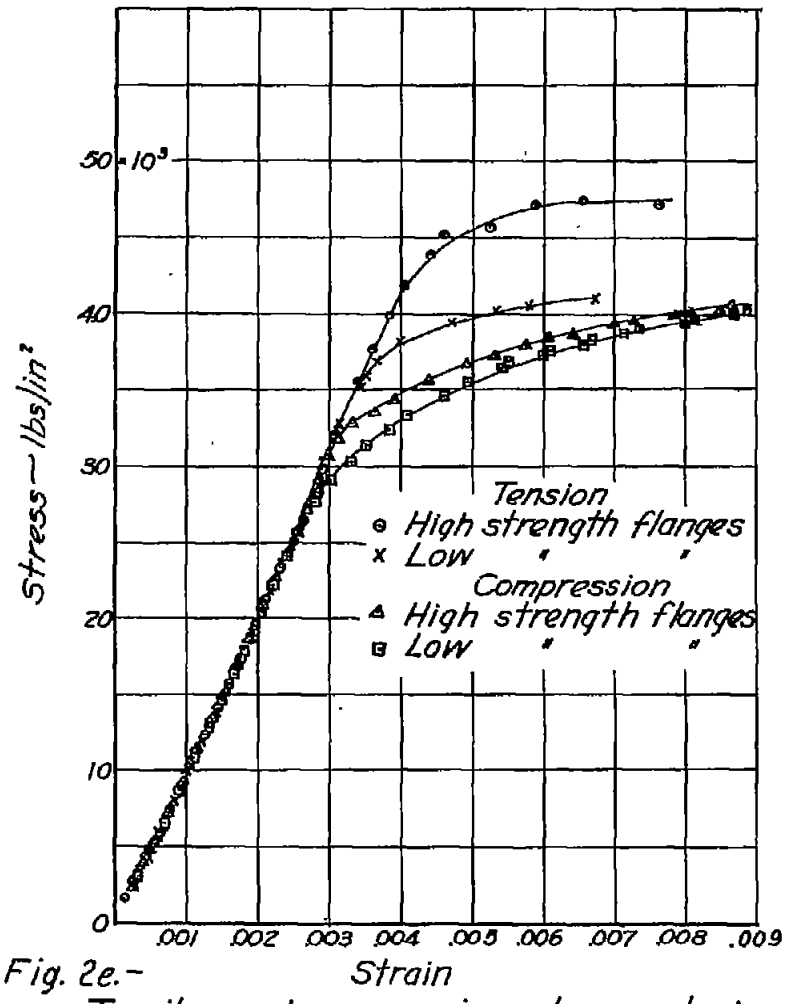

Fig. 2e.- Tensile and compressive stress-strain curve, flange material, beams E.

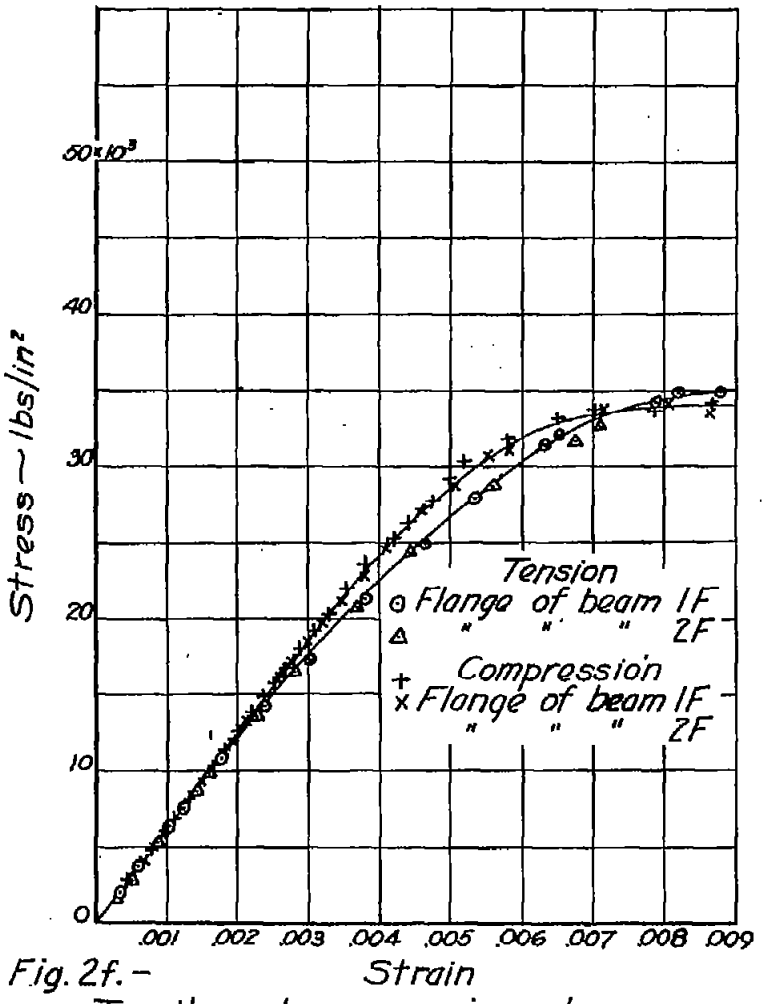

Fig. 2f.- Tensile and compressive stress-strain curve, flange material, beams F.

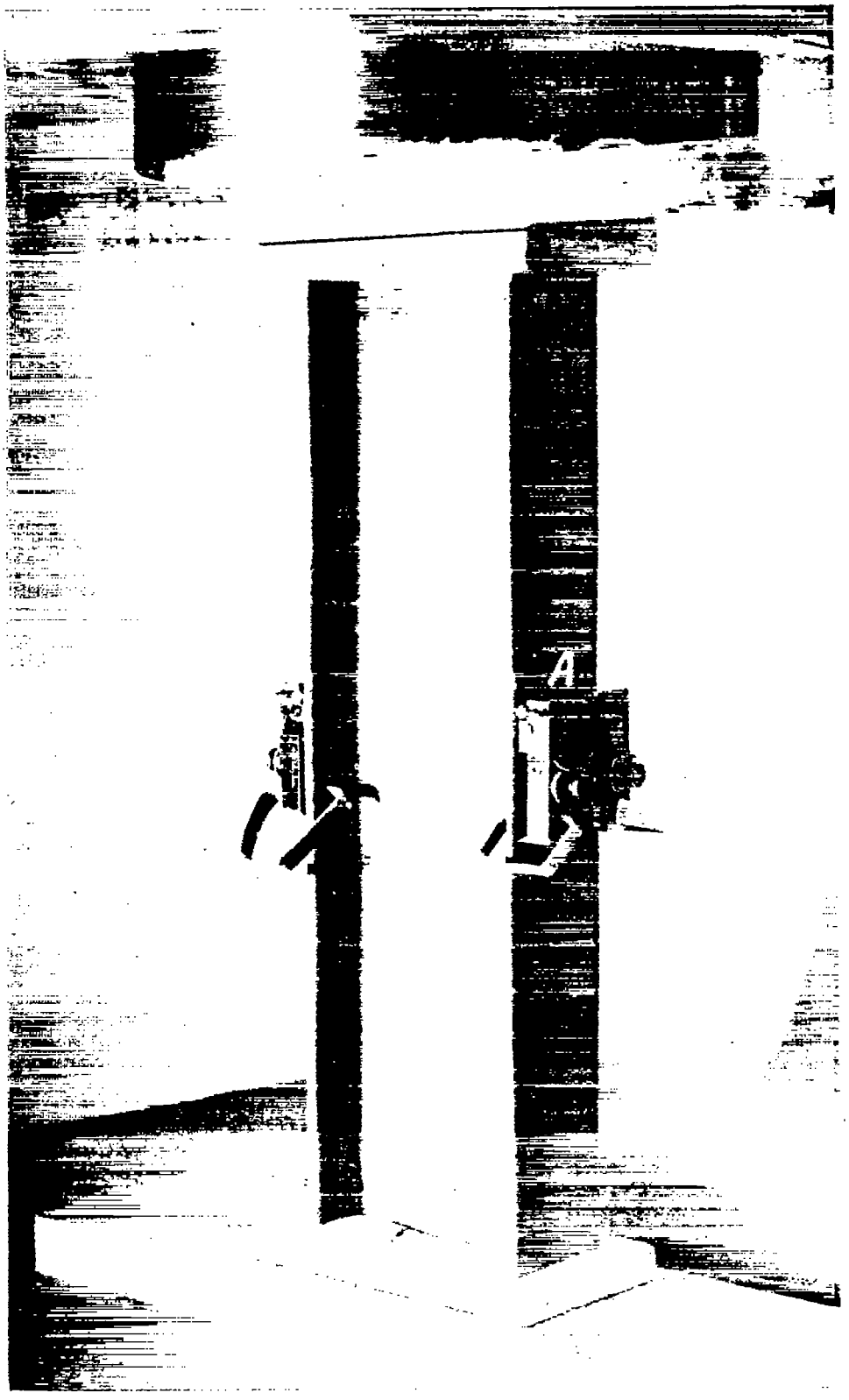

Figure 3.- Short column test of beam 1F.

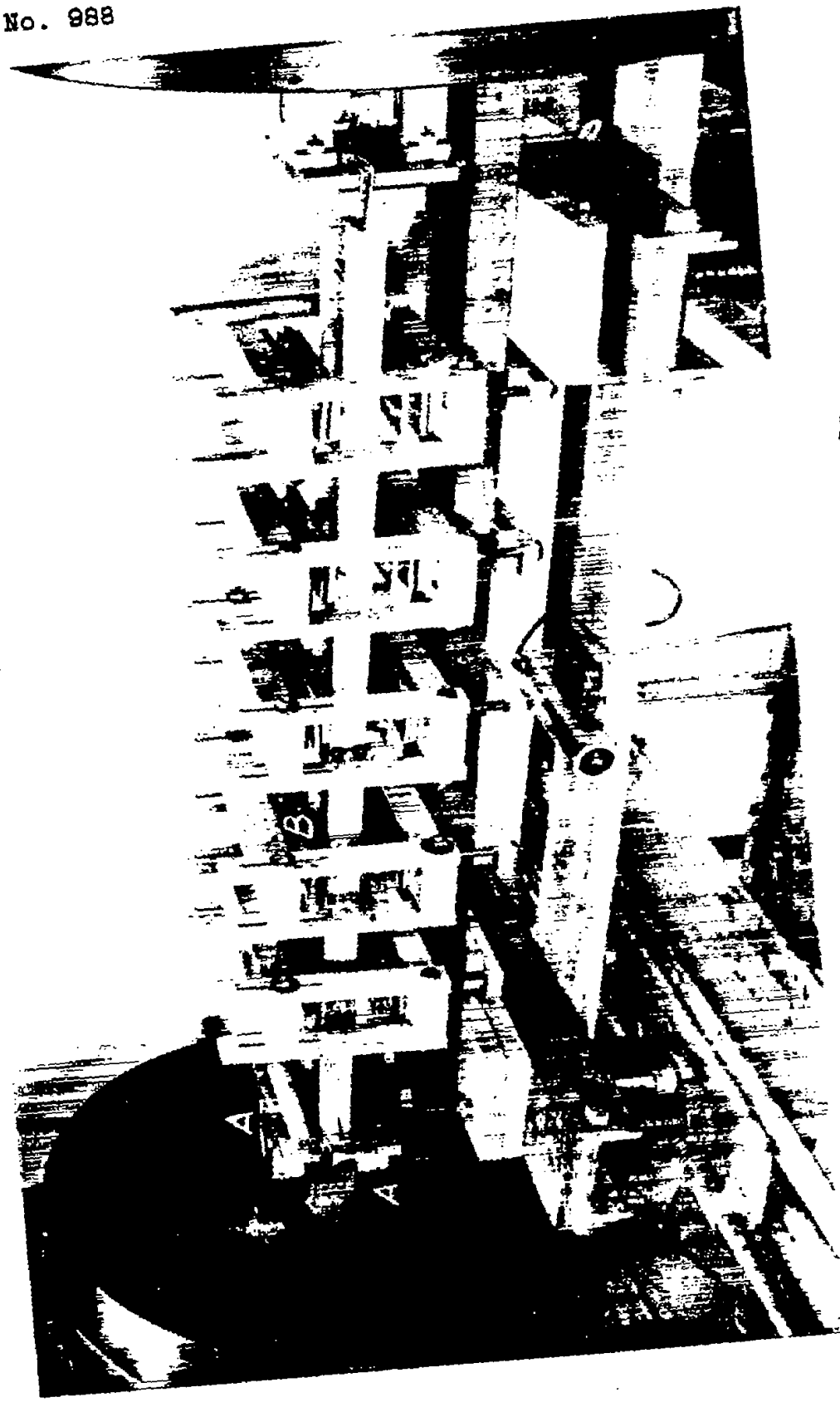

Figure 4.- Long column test of beam 2B.

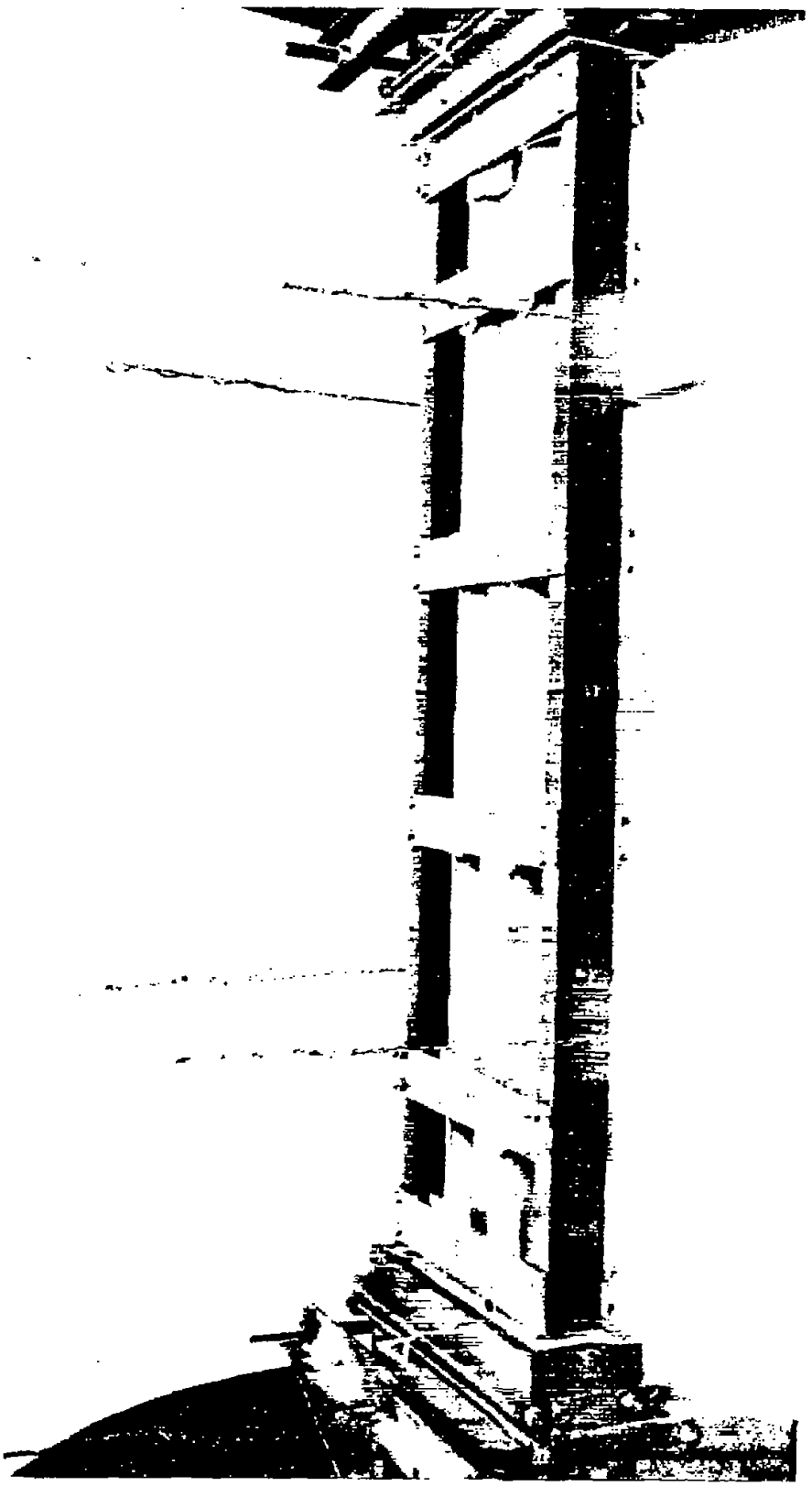

Figure 5.- Long column test of beam 2F.

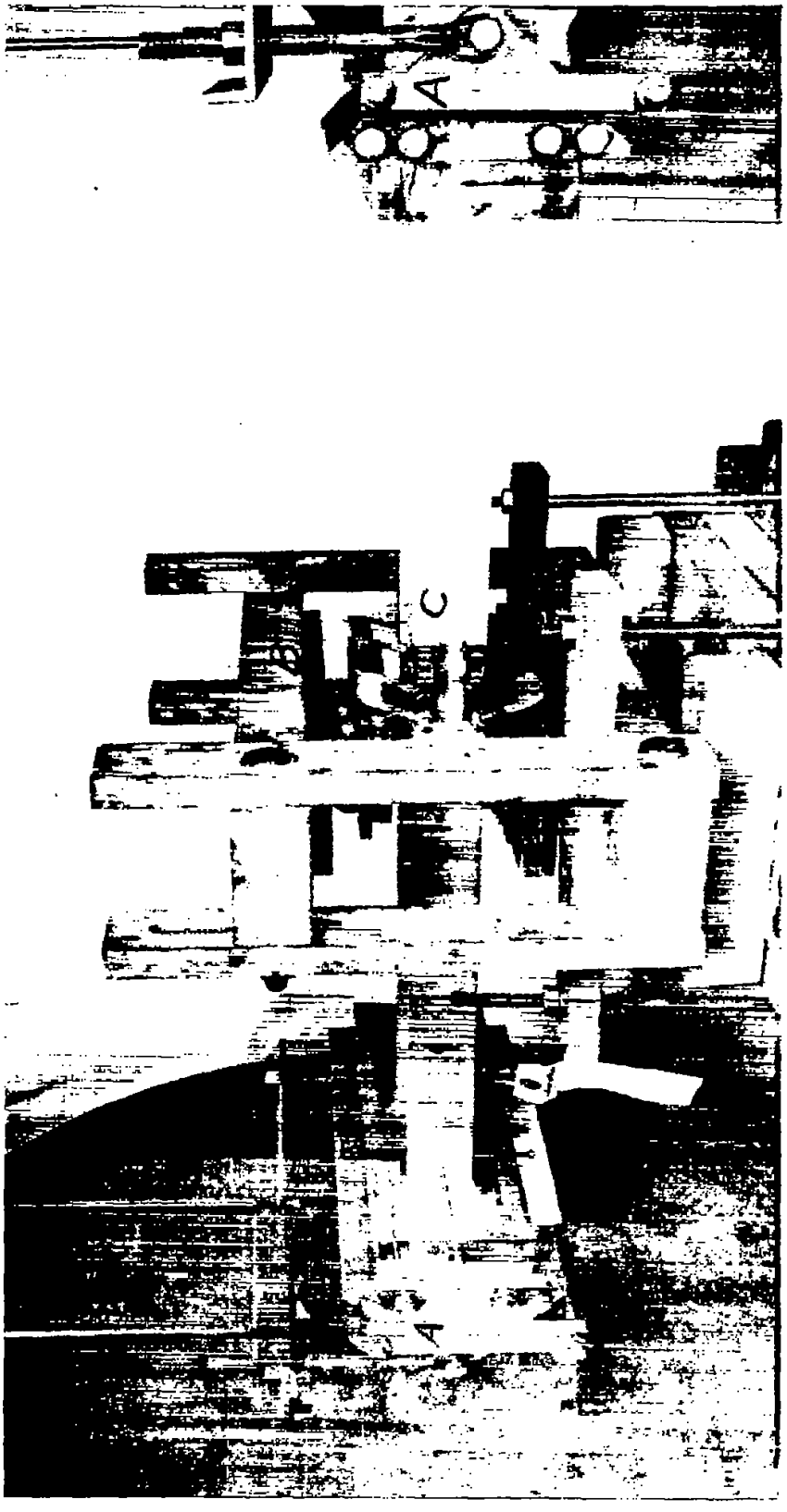

Figure 6.- Short column test of beam 1E.

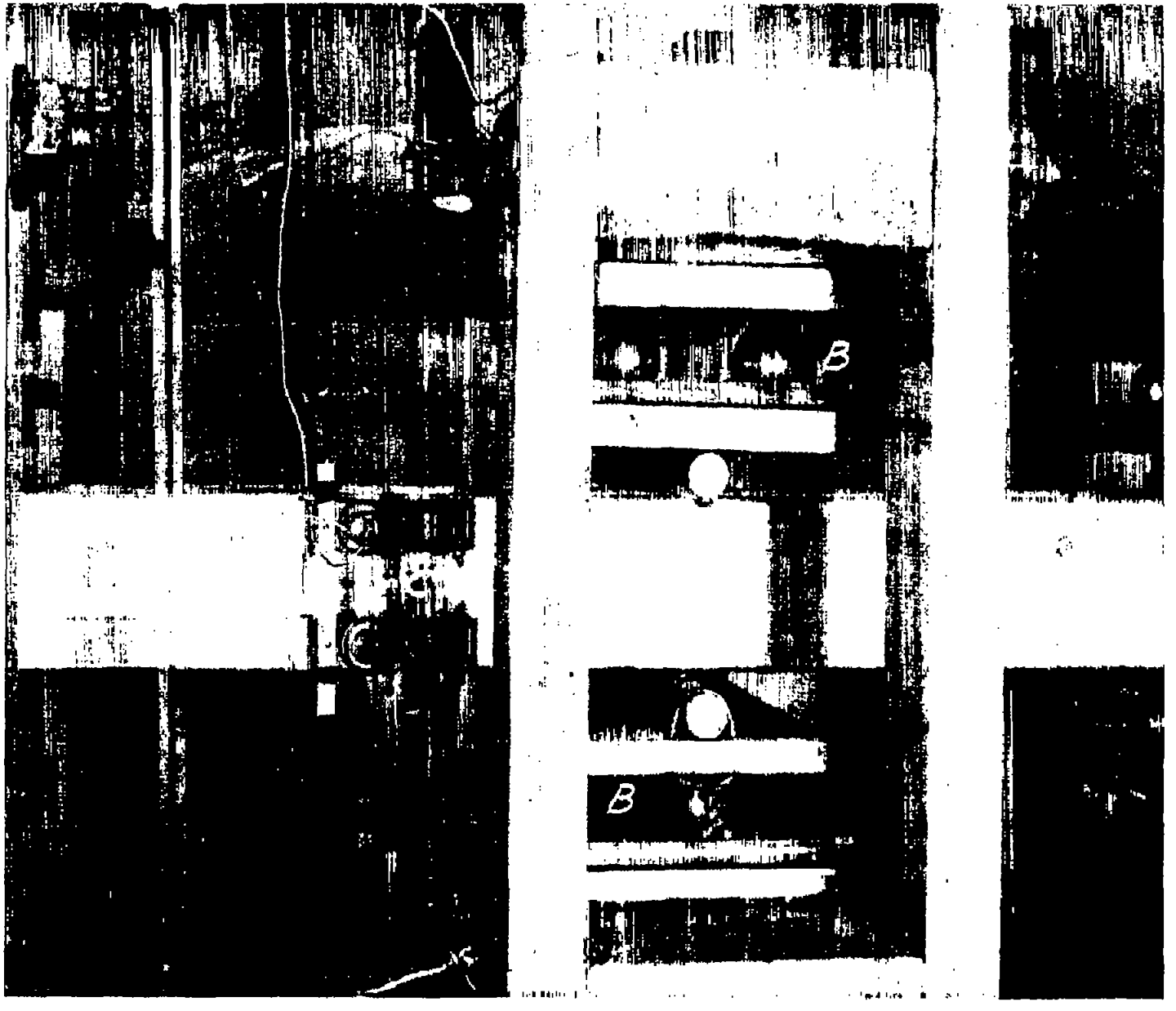

Figure 7.- Guide against lateral buckling of long column specimen 2B.

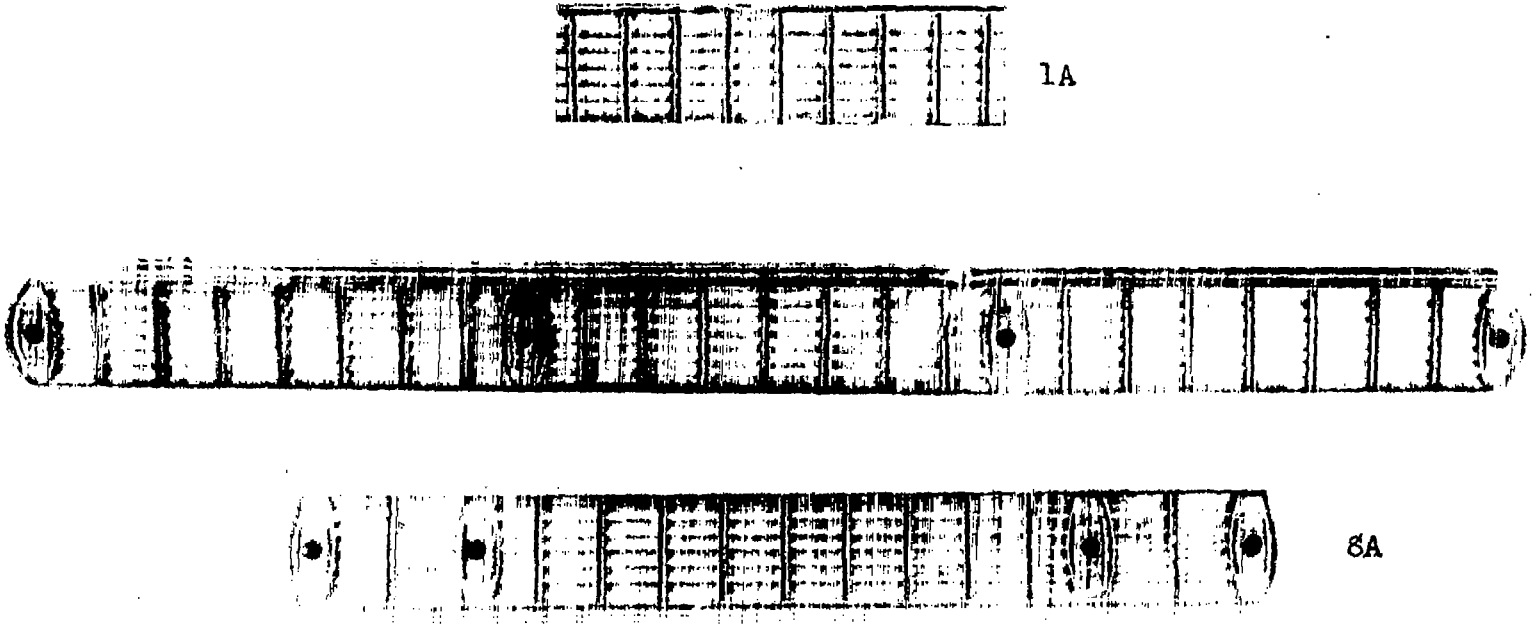

Figure 8a.- Specimens of series "A" after test.

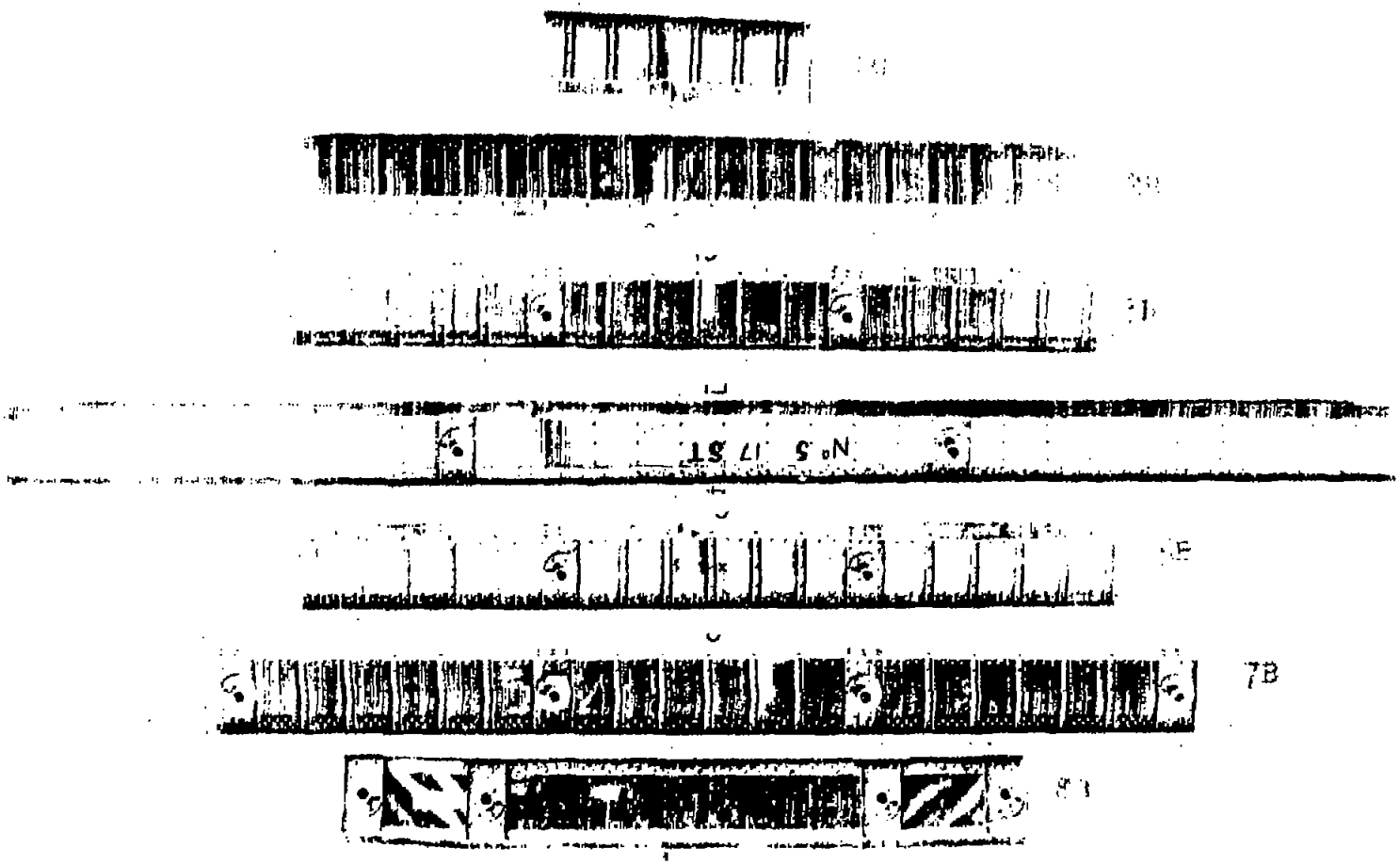

Figure 8b.- Specimens of series "B" after test.

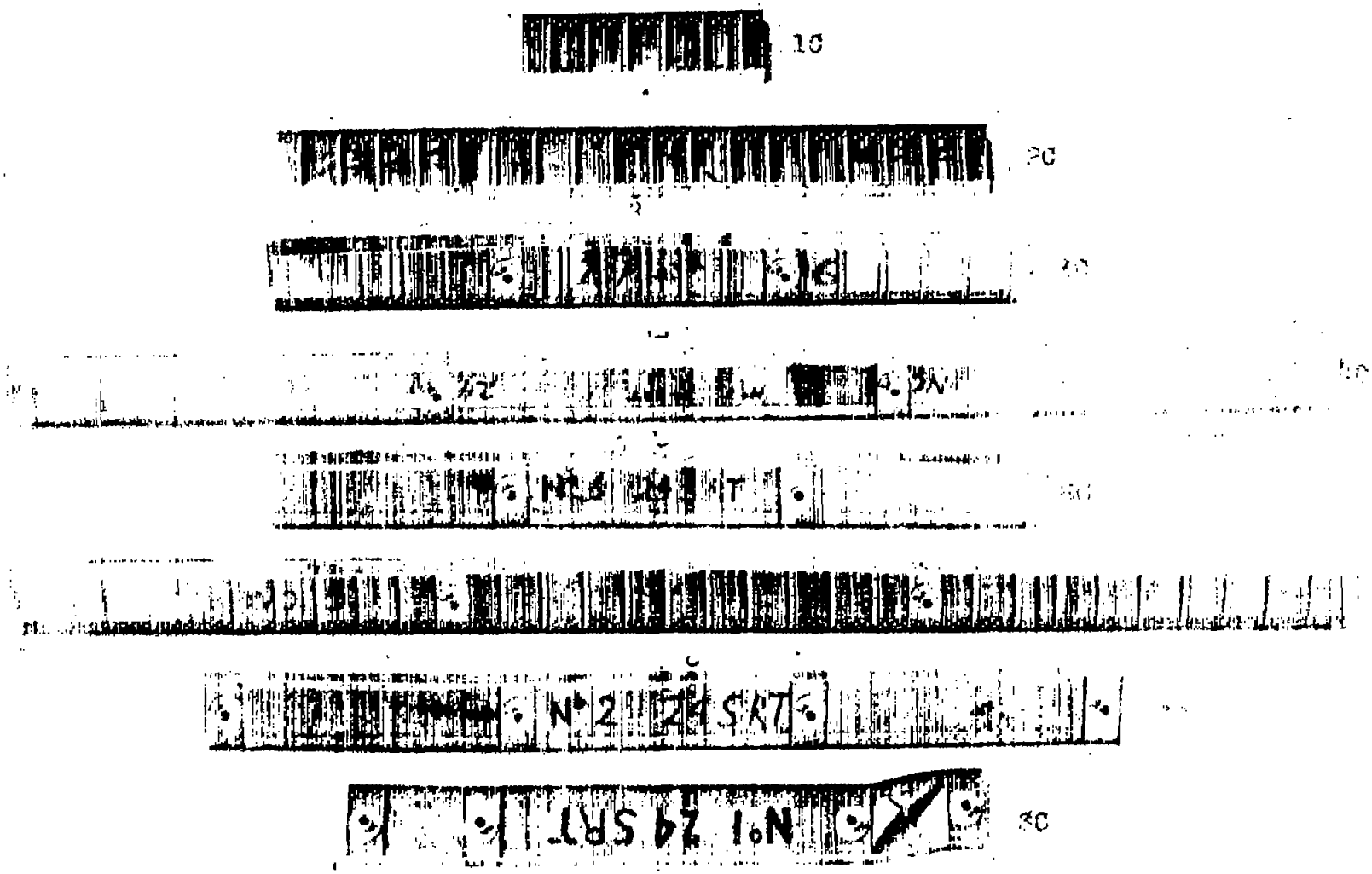

Figure 8c.- Specimens of series "C" after test.

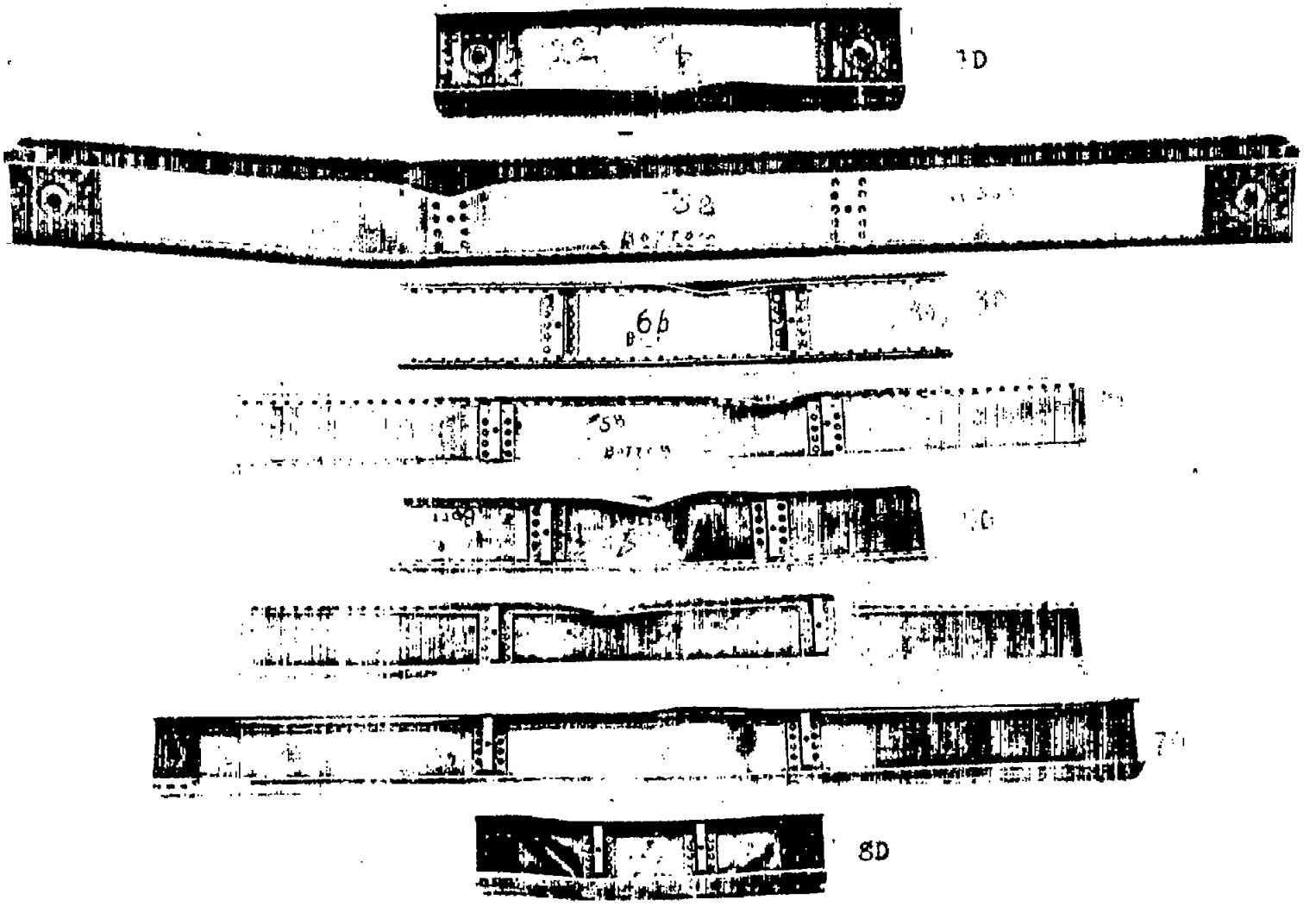

Figure 8d.- Specimens of series "D" after test.

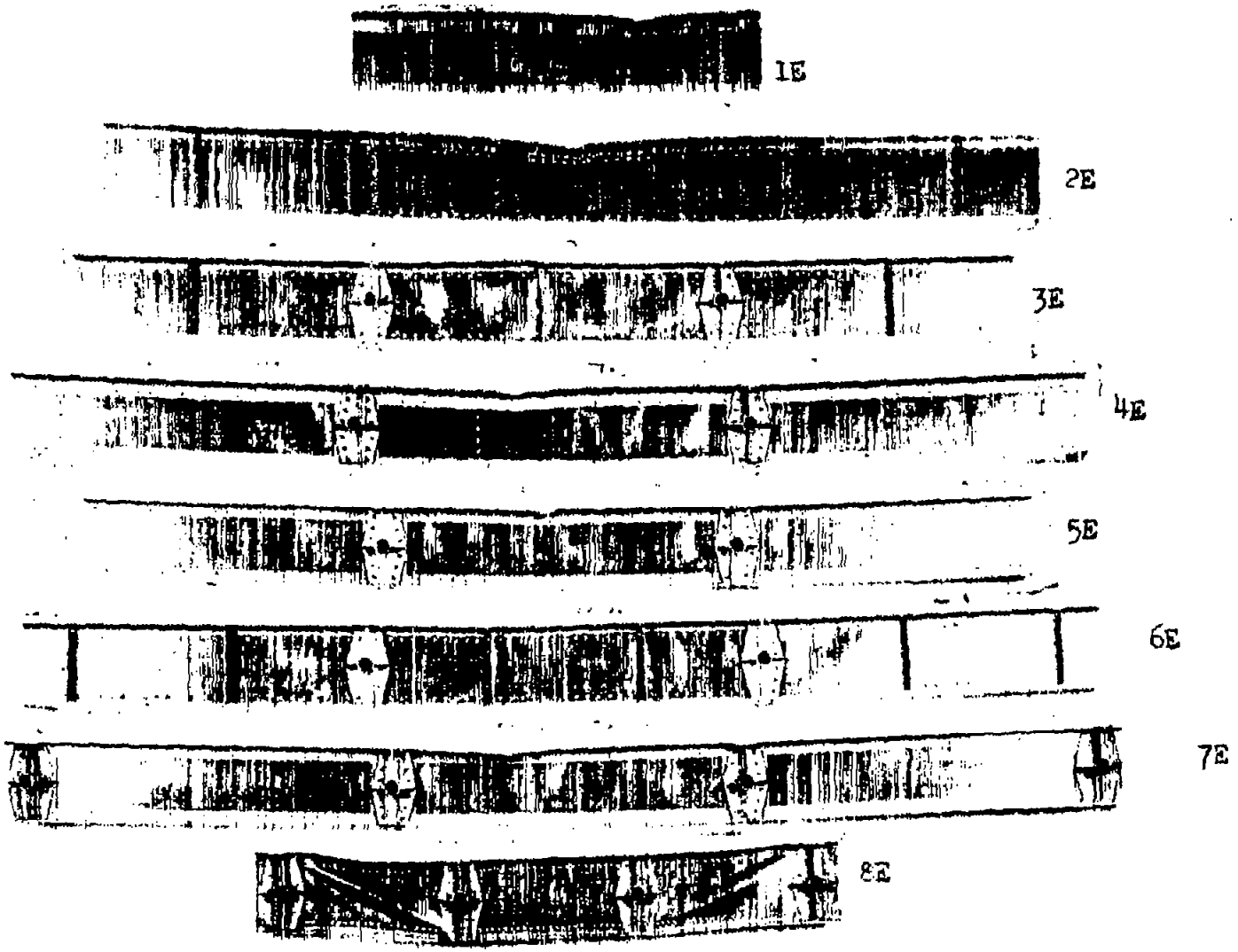

Figure 8e.- Specimens of series "E" after test.

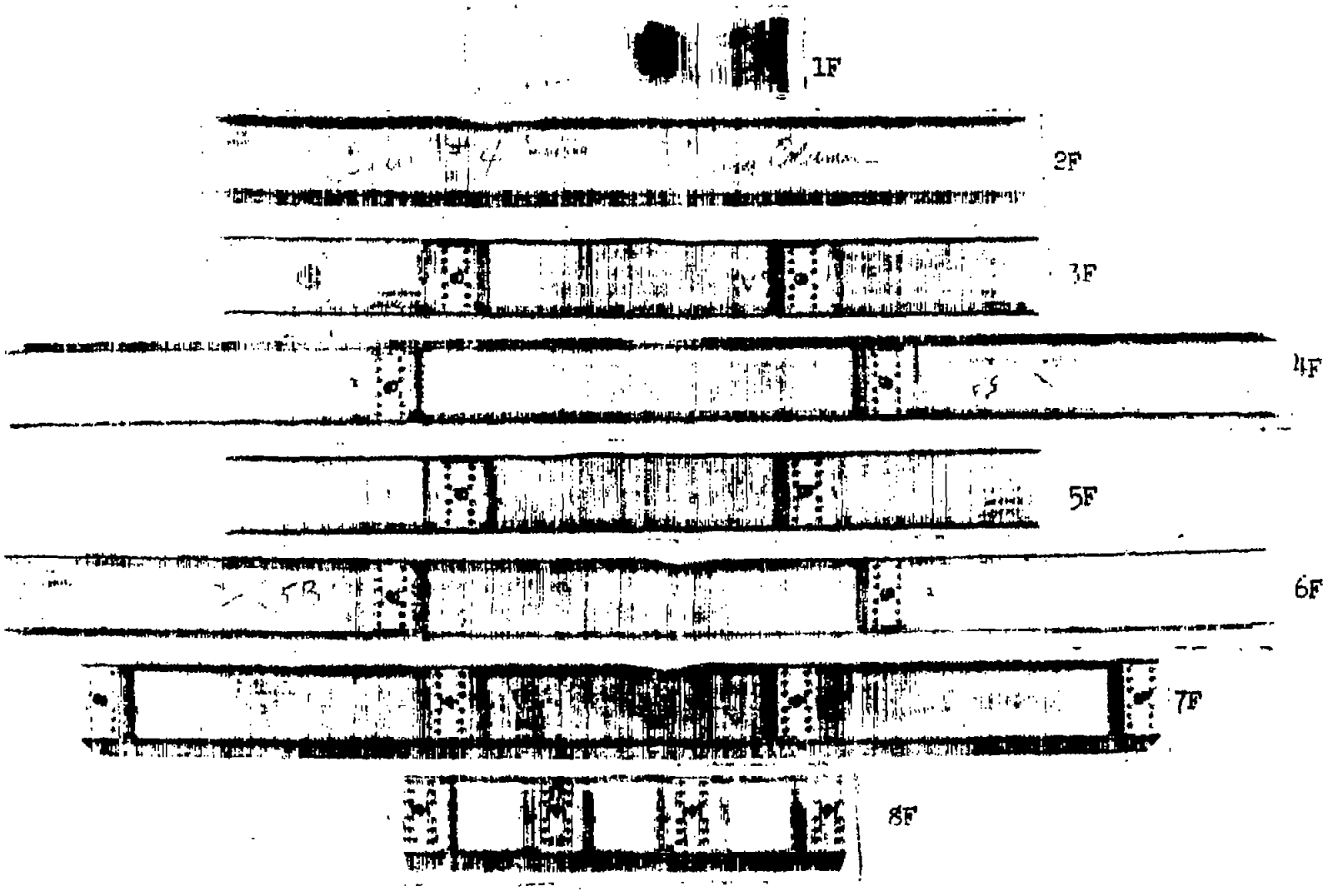

Figure 8f.- Specimens of series "F" after test.

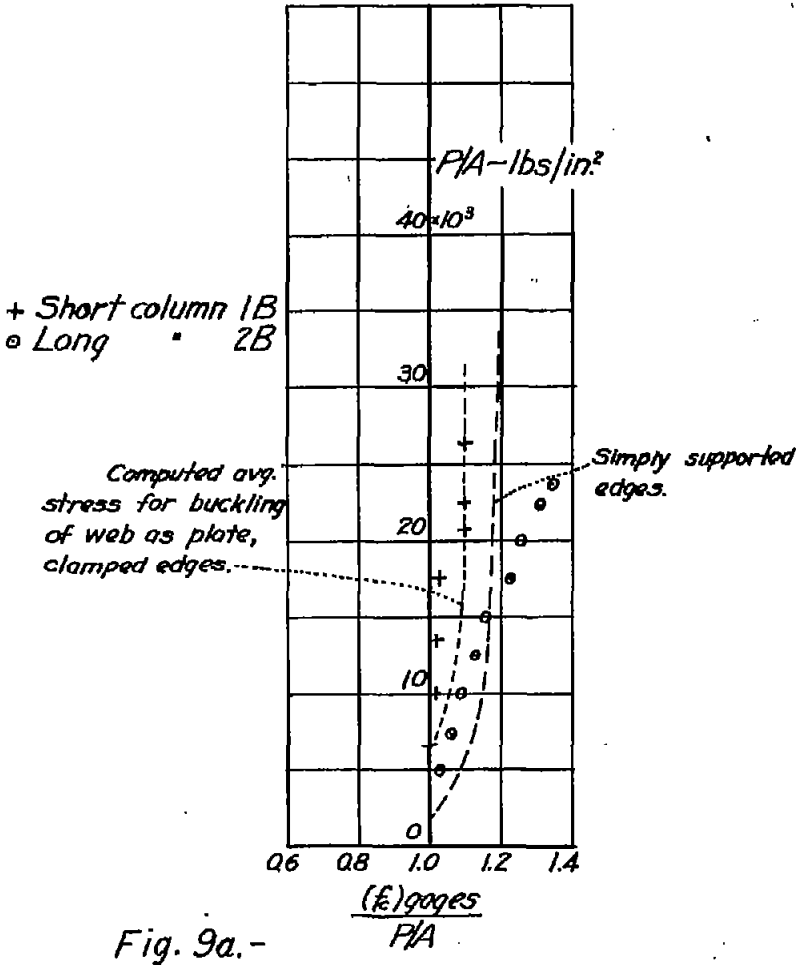

Fig. 9a.- Axial tests, specimens of series B

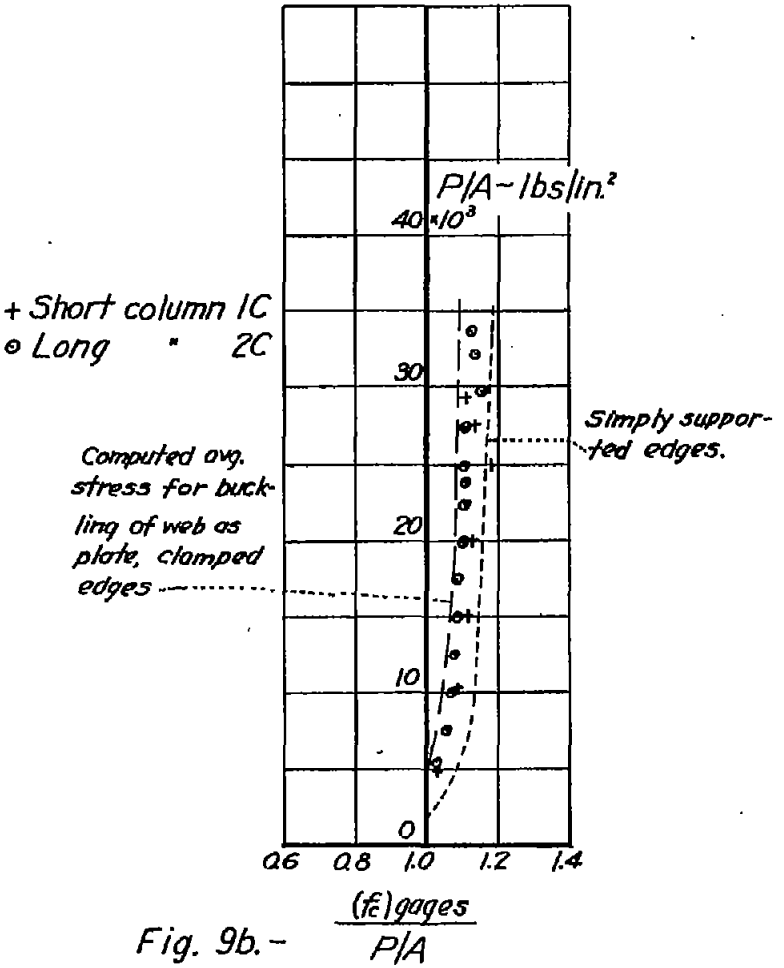

Fig. 9b.- Axial tests, specimens of series C.

+ Short column 1D
⊙ Long column 2D

Computed avg. stress for buckling of web as plate, ———— clamped edges
---------- simply supported edges

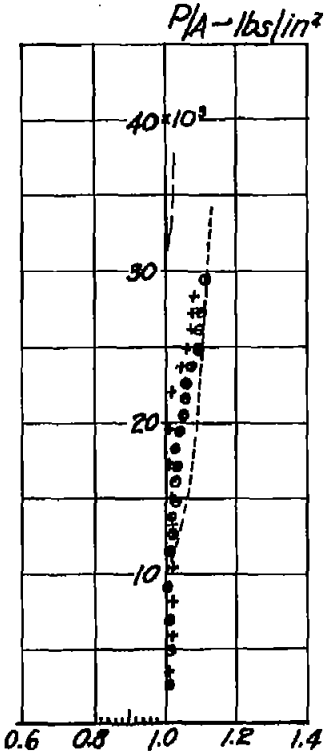

Fig. 9c.- Axial tests, specimens of series D

+ Short column 1E
⊙ Long column 2E

Computed avg. stress for buckling of web as plate, ———— clamped edges
---------- simply supported edges

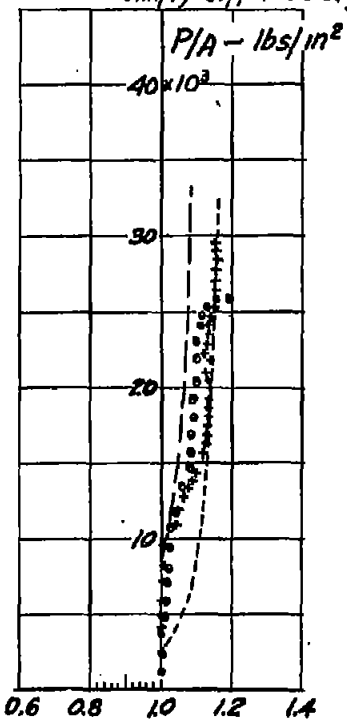

Fig. 9d.- Axial test, specimens of series E.

+ Short column 1F
⊙ Long column 2F

Computed avg. stress for buckling of web as plate, ———— clamped edges
---------- simply supported edges

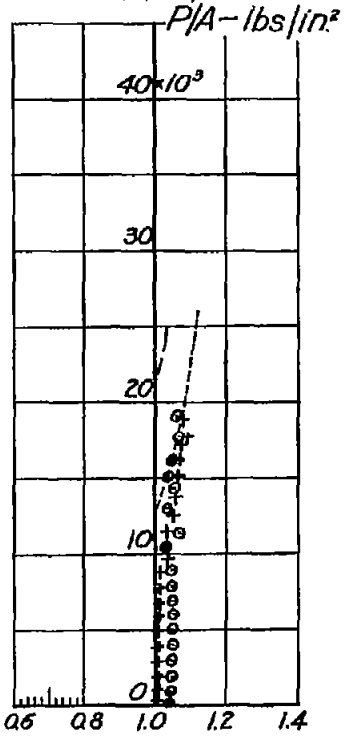

Fig. 9e.- Axial tests, specimens of series F.

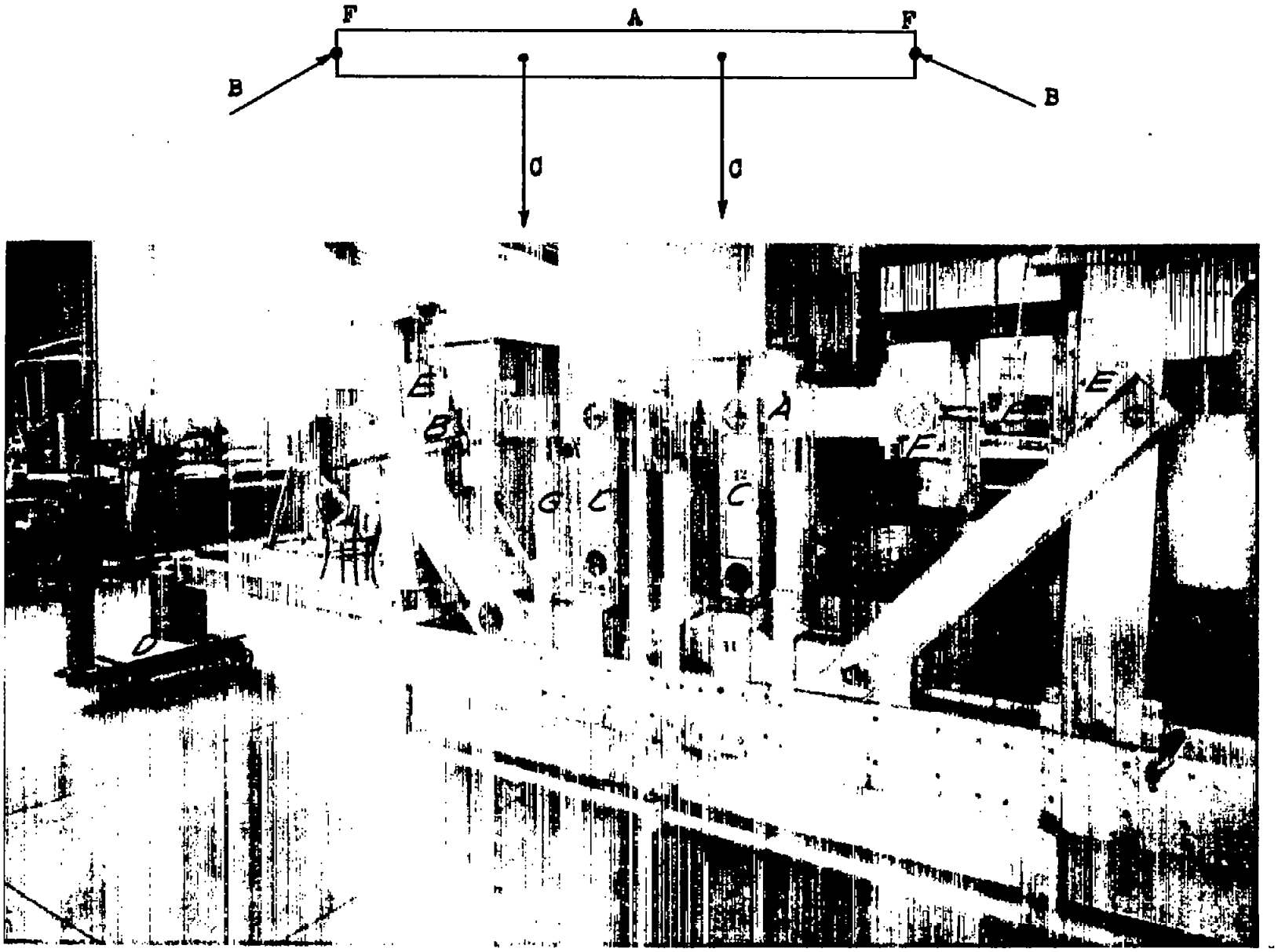

Figure 10.- Machine for combined load tests of specimens of types A, B, C, and of specimens 4D, 6D.

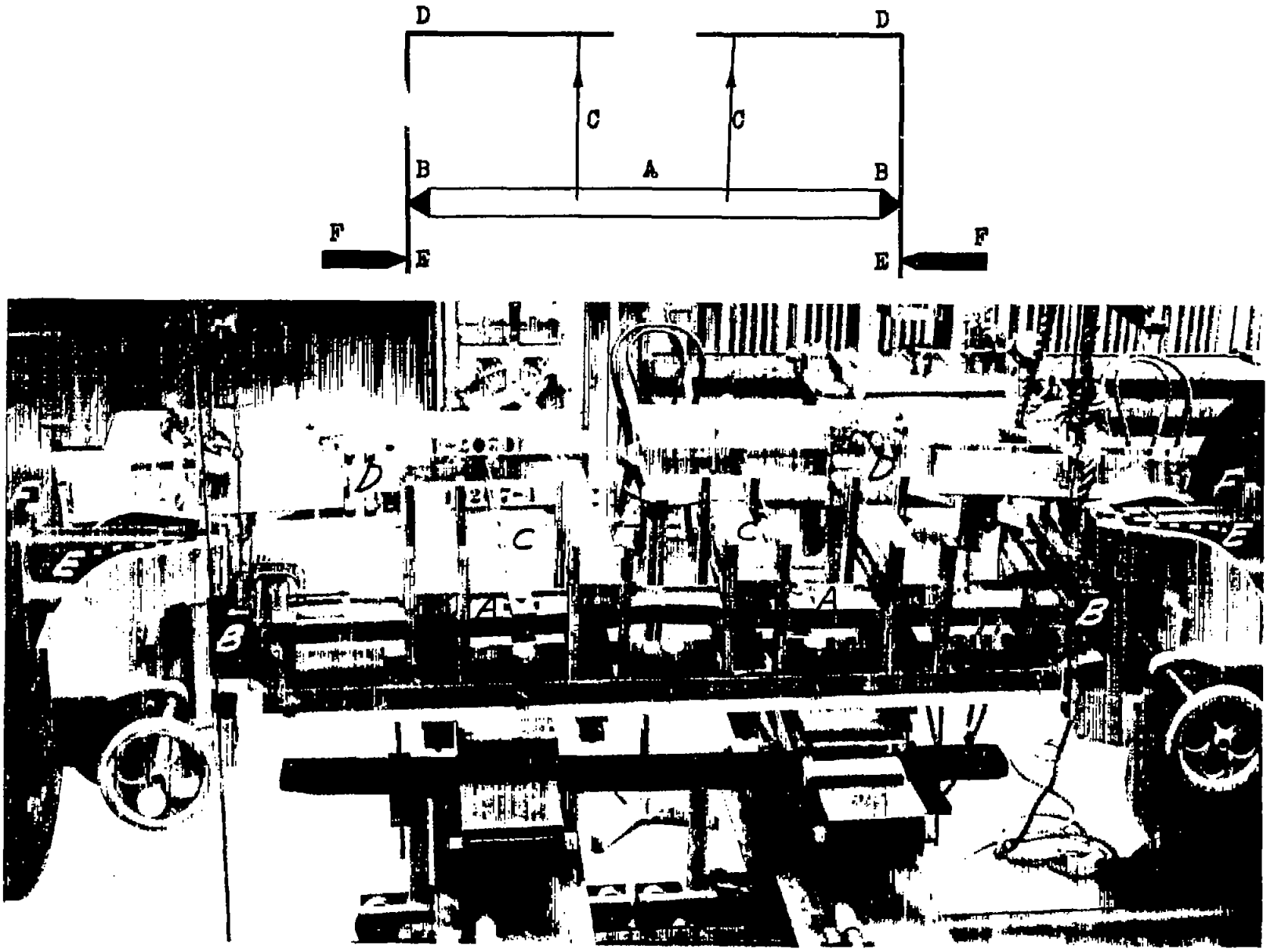

Figure 11.- Fixture for combined load tests of specimens of types E, F, and of specimens 3D, 5D.

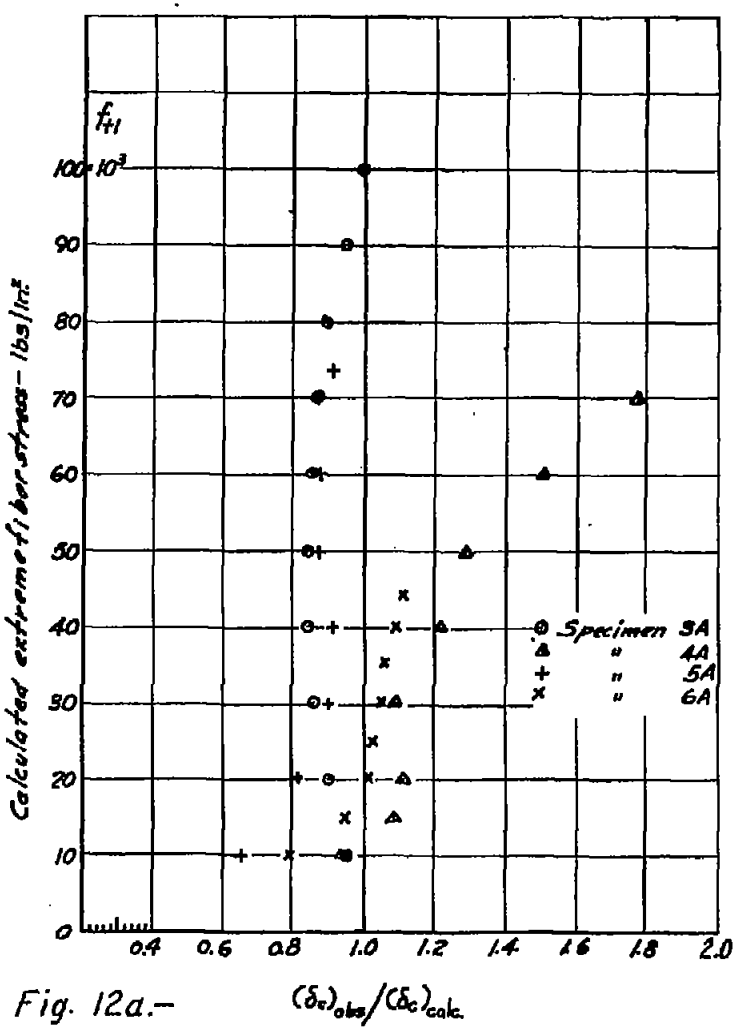

Fig. 12a.- Comparison of observed and calculated center deflections under combined load, specimens of type A.

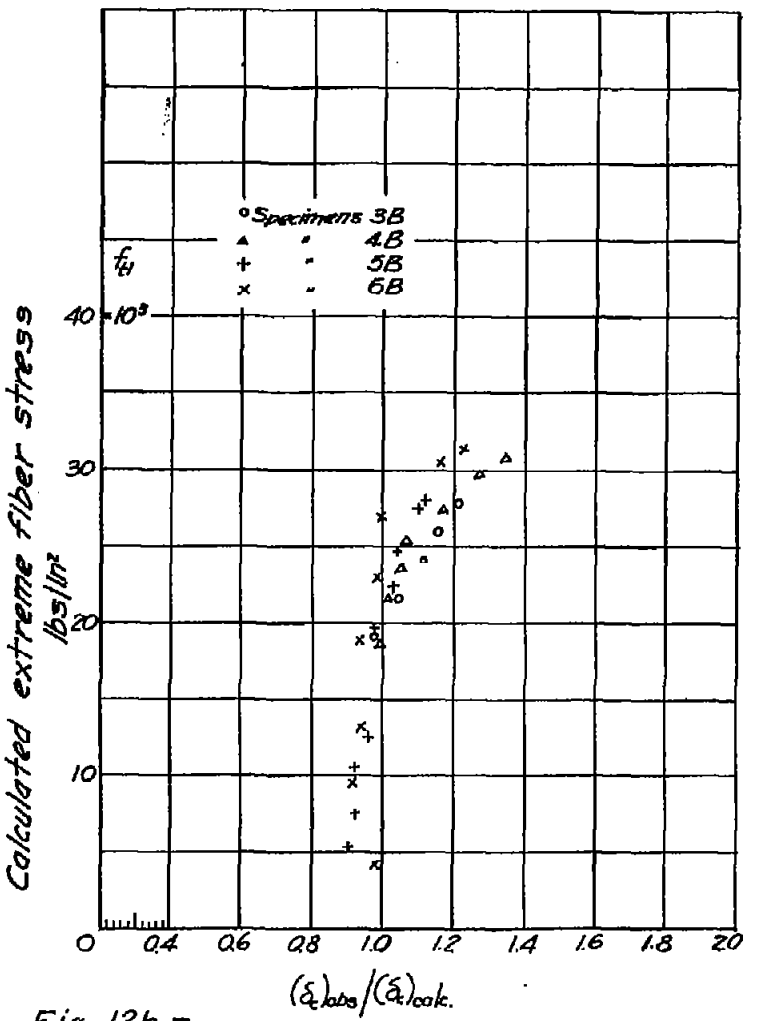

Fig. 12b.- Comparison of observed and calculated center deflections under combined load, specimens of type B.

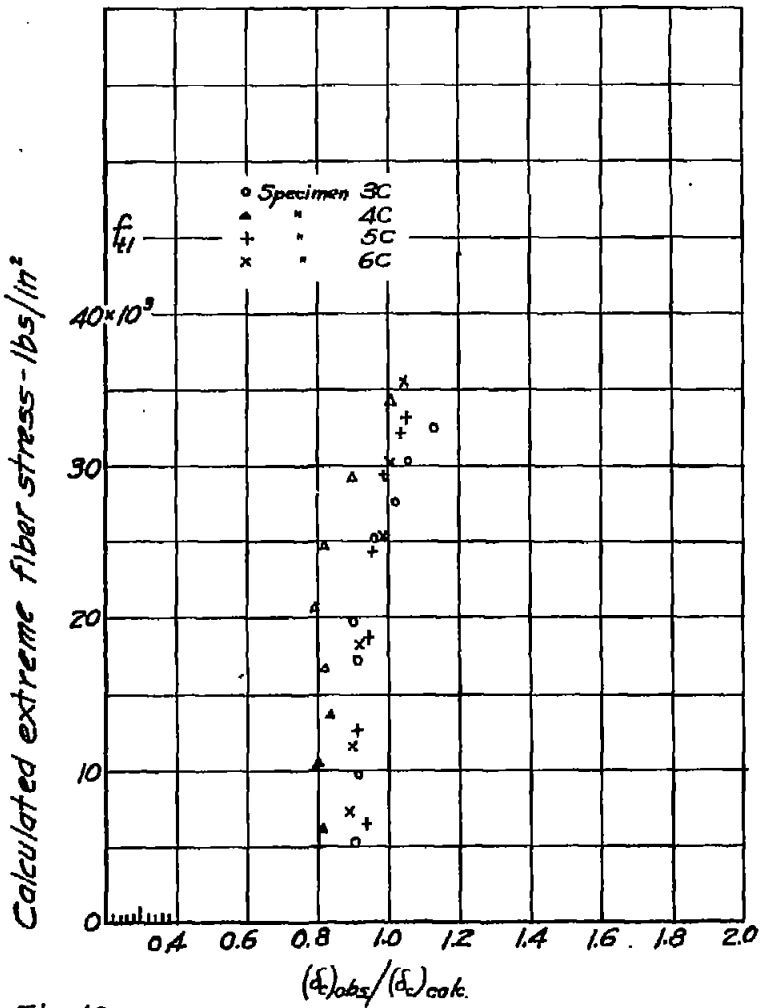

Fig. 12c.-

Comparison of observed and calculated center deflections under combined load, specimens of type C.

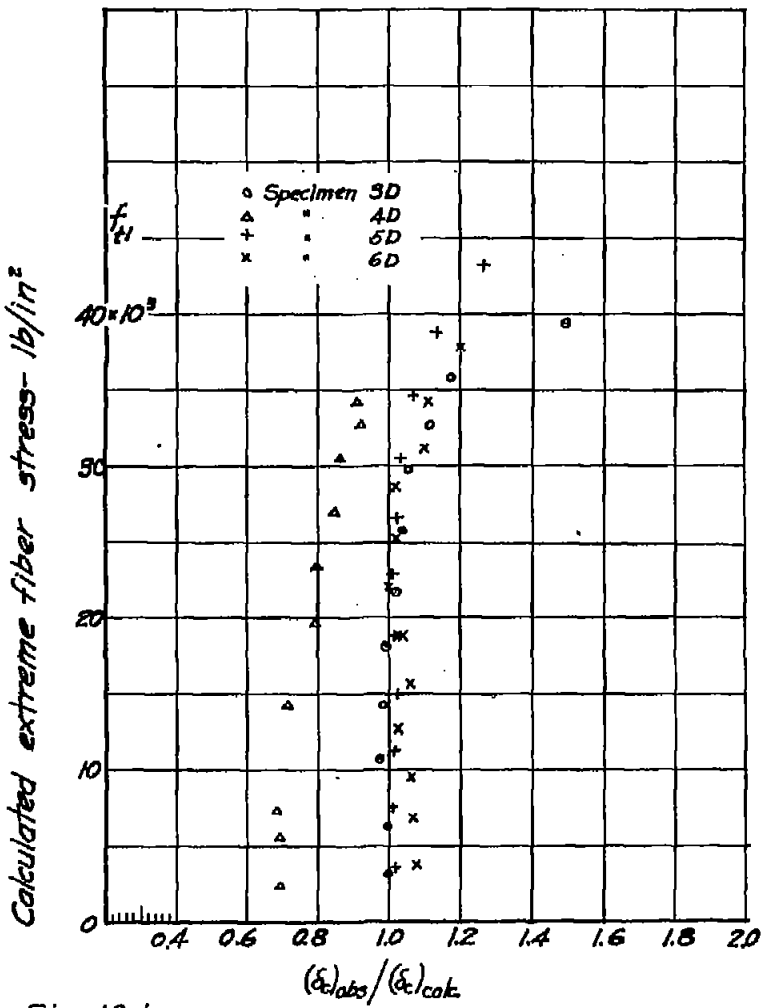

Fig. 12d.-

Comparison of observed and calculated center deflections under combined load, specimens of type D.

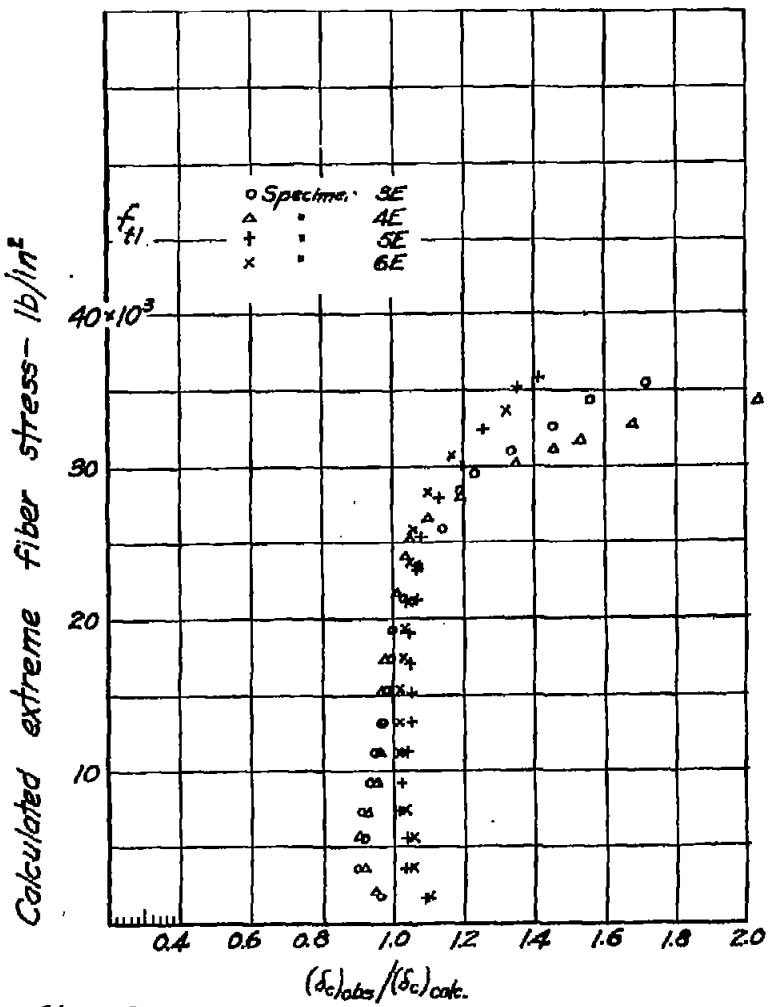

Fig. 12e.- Comparison of observed and calculated center deflections under combined load, specimens of type E.

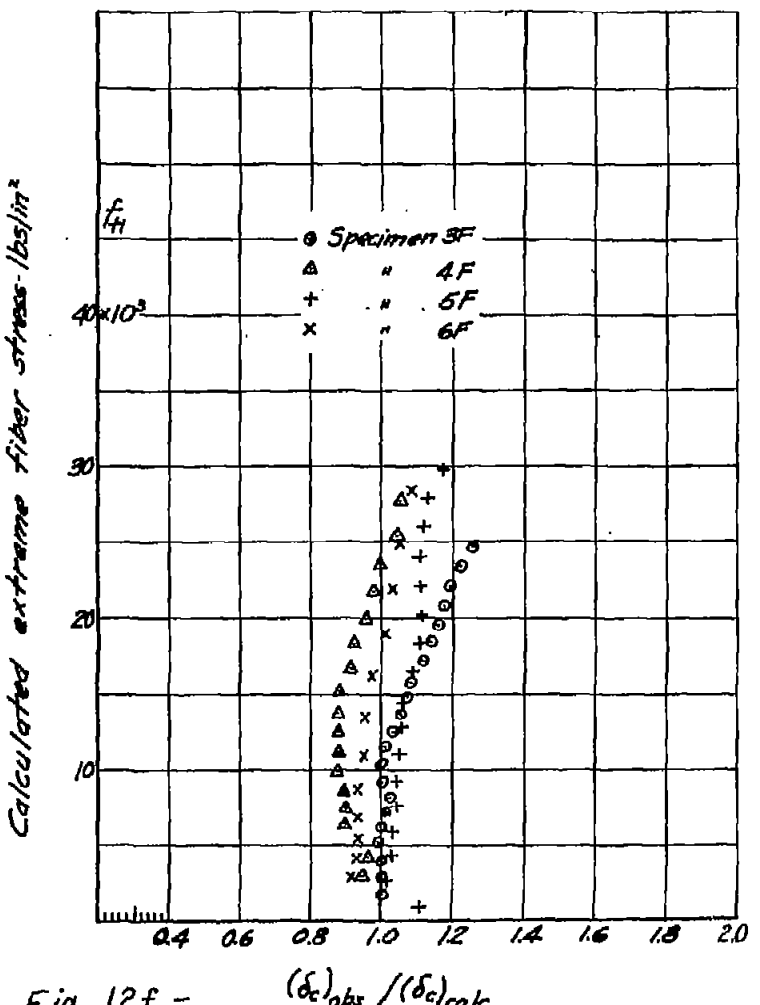

Fig. 12f.- Comparison of observed and calculated center deflections under combined loads, specimens of type F.

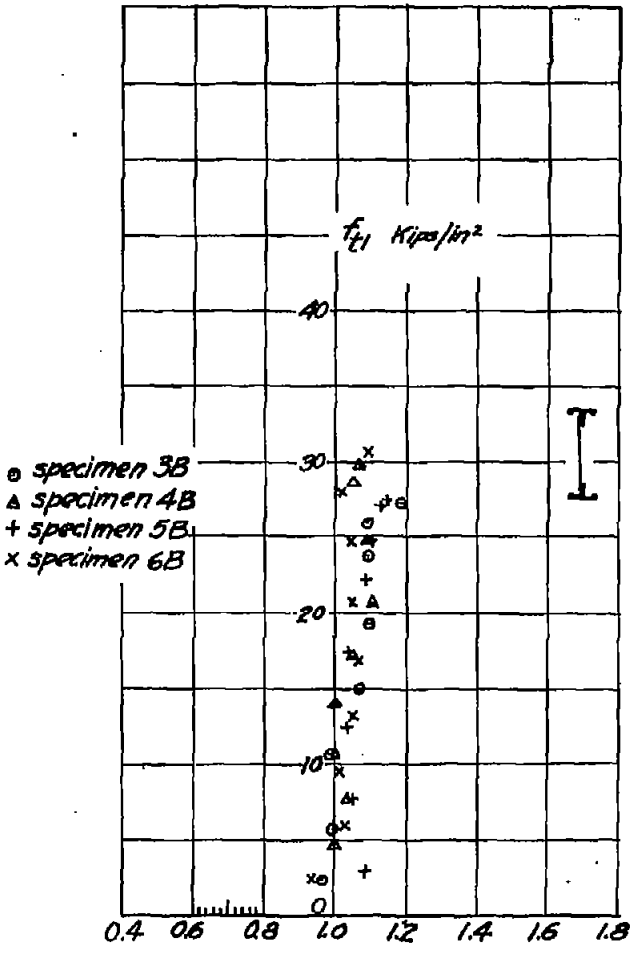

Fig. 13a. – f_{t3}/f_{t1}

Comparison of measured extreme fiber stress, f_{t3}, and theoretical extreme fiber stress, f_{t1}, for specimens of type B under combined load.

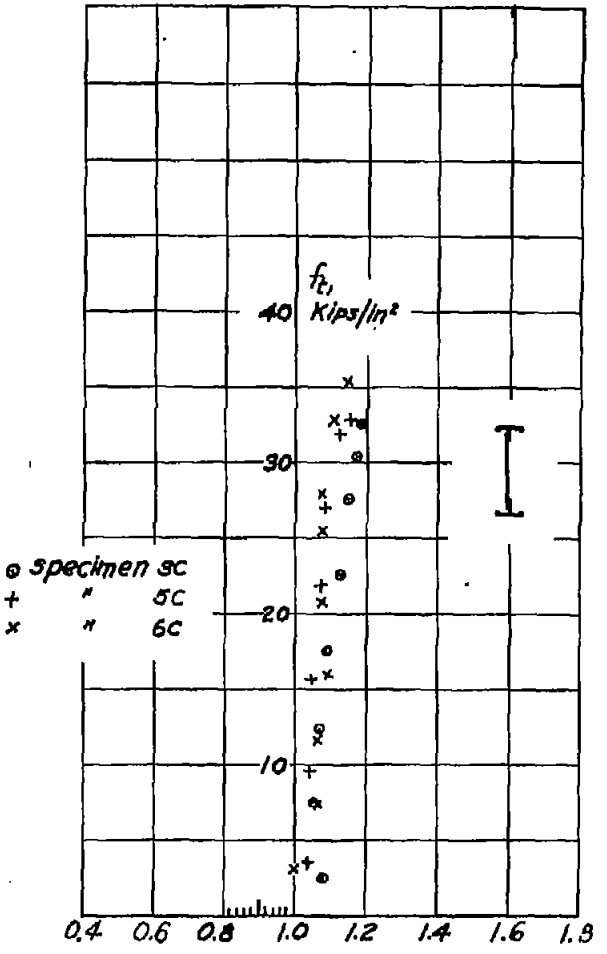

Fig. 13b. – f_{t3}/f_{t1}

Comparison of measured extreme fiber stress, f_{t3}, and theoretical extreme fiber stress, f_{t1}, for specimens of type C under combined load.

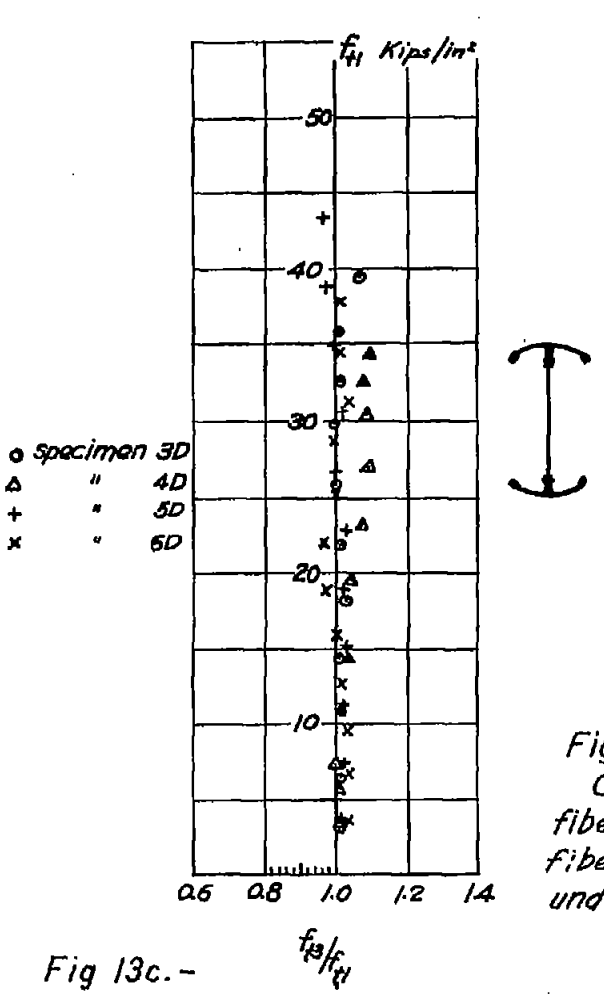

Fig 13c.- Comparison of measured extreme fiber stress, f_{t3}, and theoretical extreme fiber stress, f_{t1}, for specimens of type D under combined loads.

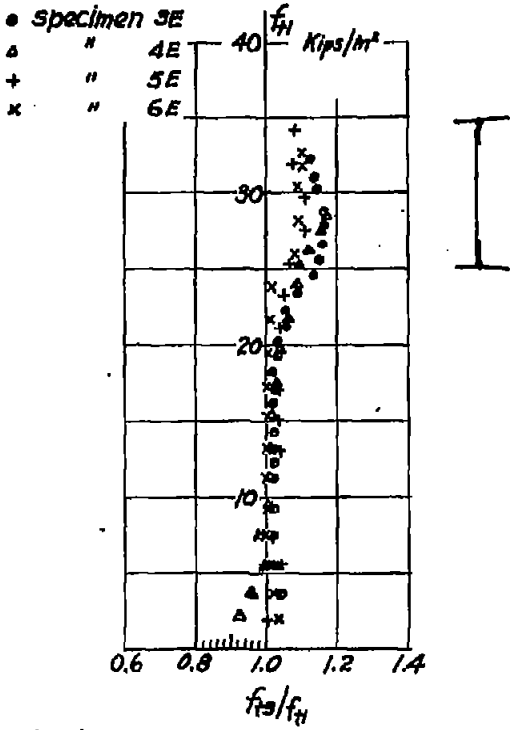

Fig. 13d.- Comparison of measured extreme fiber stress, f_{t3}, and theoretical extreme fiber stress, f_{t1}, for specimens of type E under combined load.

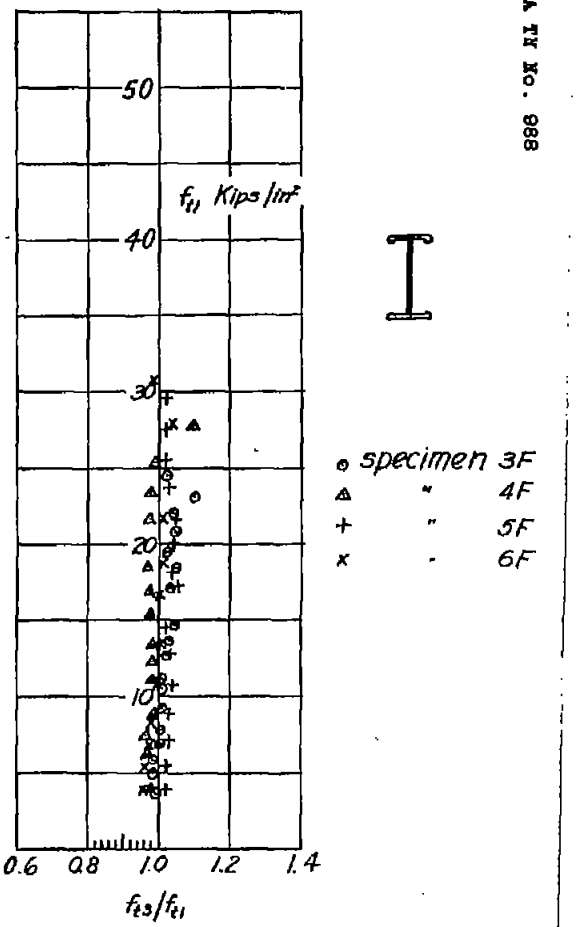

Fig. 13e.- Comparison of measured extreme fiber stress, f_{t3}, and theoretical extreme fiber stress, f_{t1}, for specimens of type F under combined load.

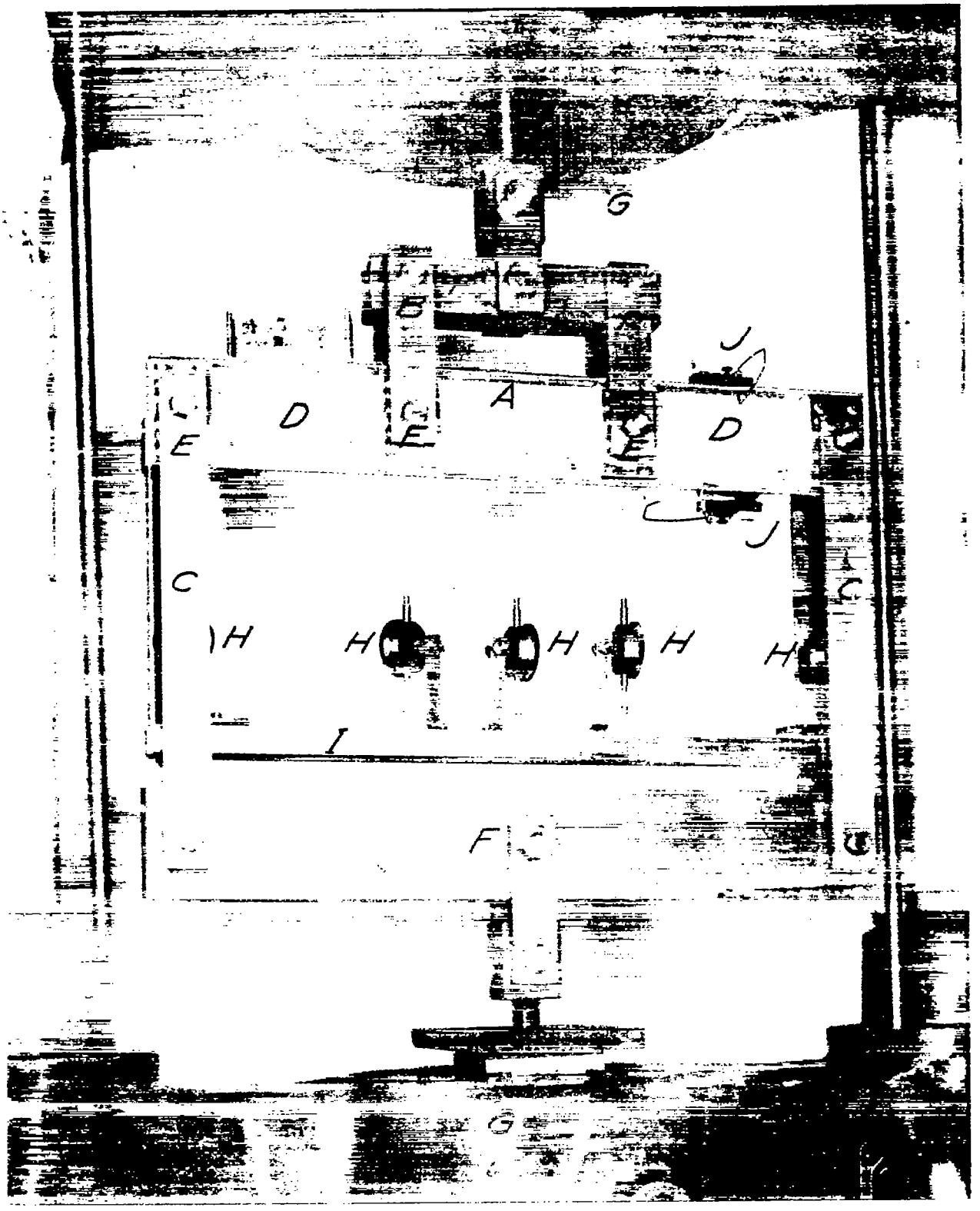

Figure 14.- Transverse load test of specimen 8F.

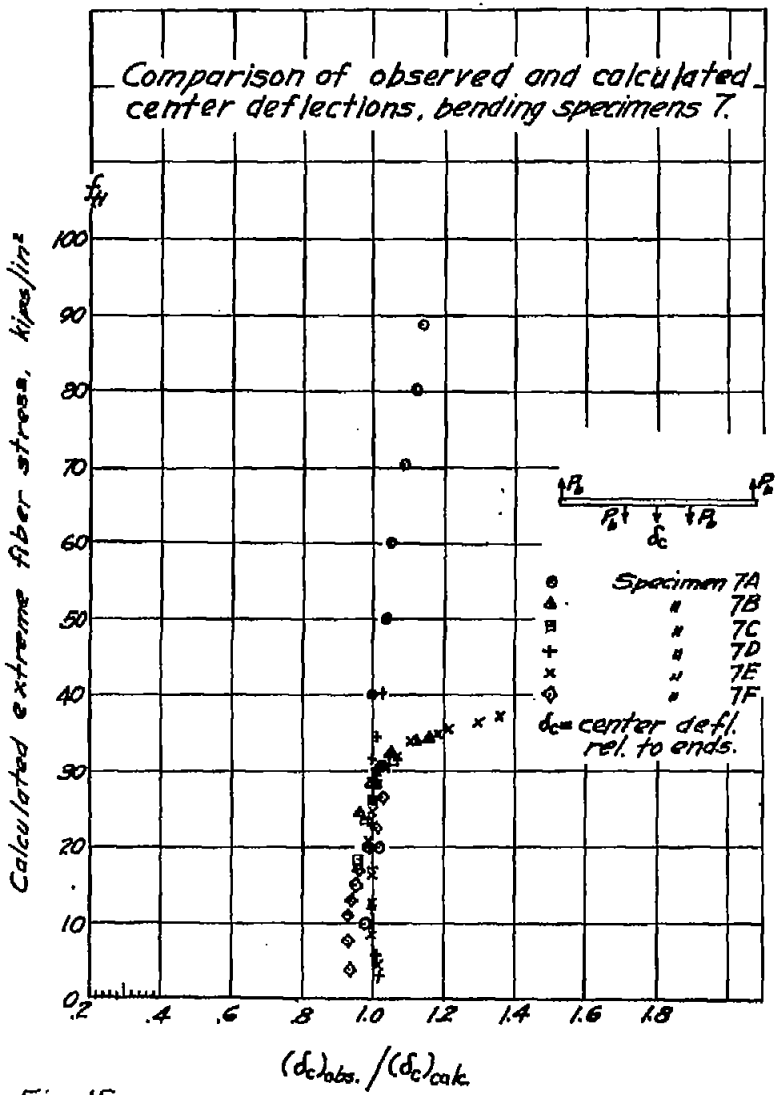

Fig. 15.

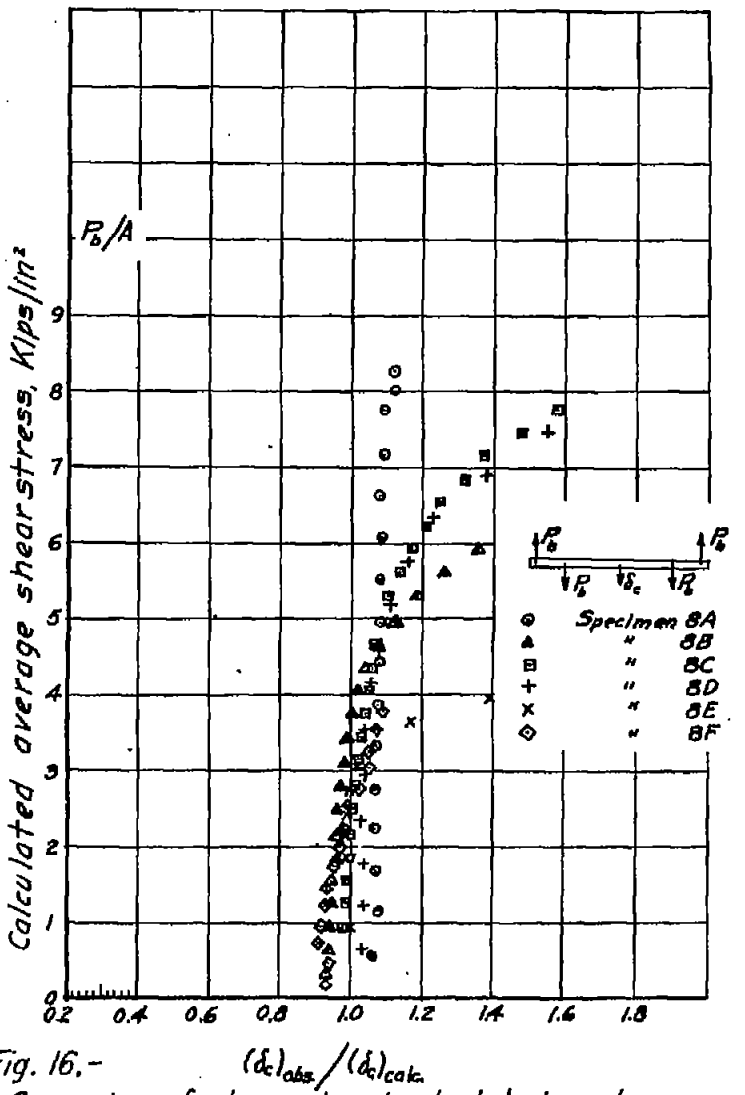

Fig. 16.- Comparison of observed and calculated center deflection, shear specimen 8.

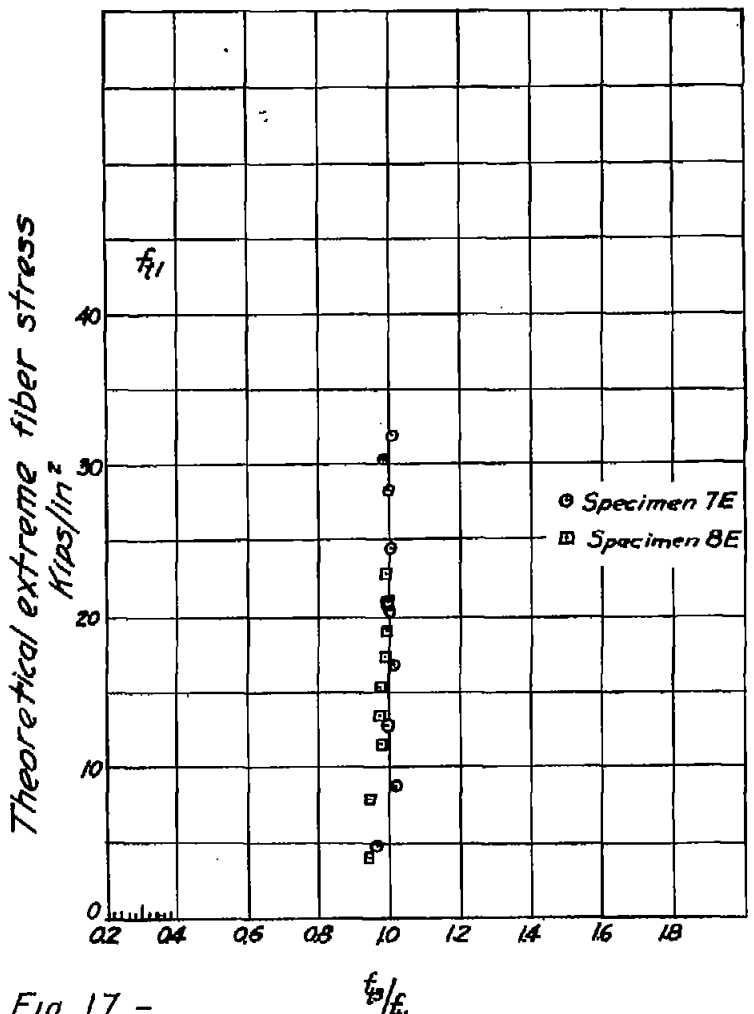

Fig. 17.- Comparison of observed and calculated extreme fiber stresses at center, bending specimens 7E & 7F

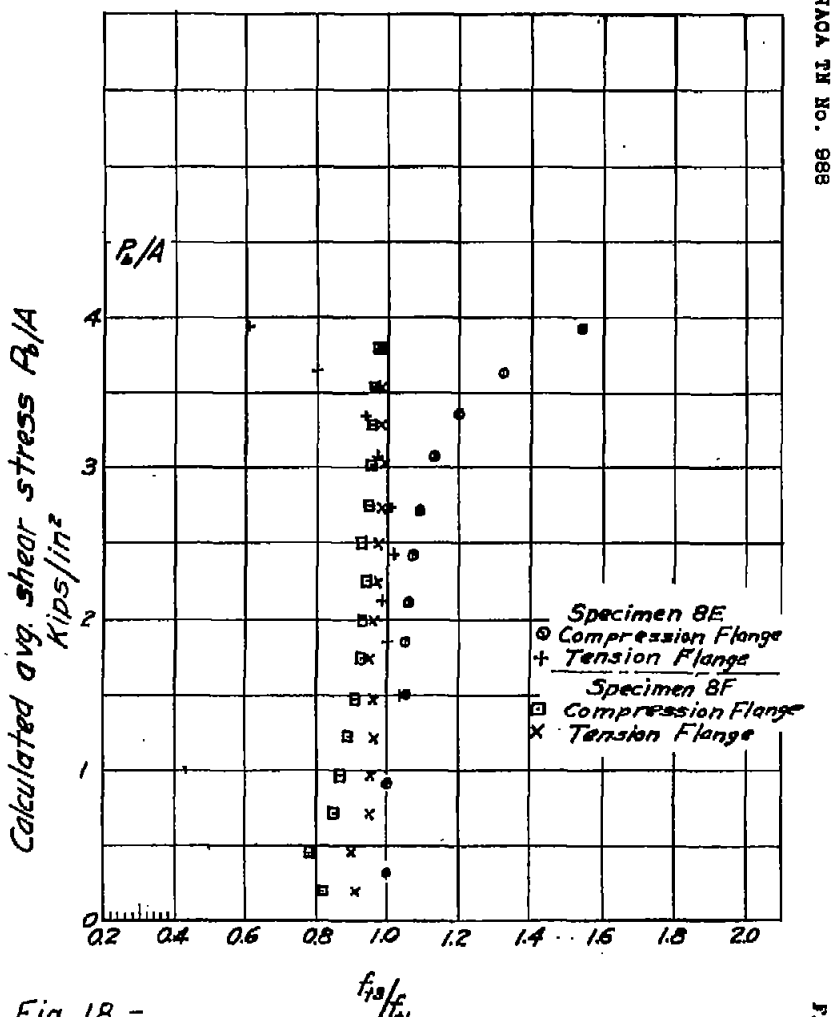

Fig. 18.- Comparison of observed and calculated extreme fiber stresses 5.32 in. from end pin, shear specimen 8E.

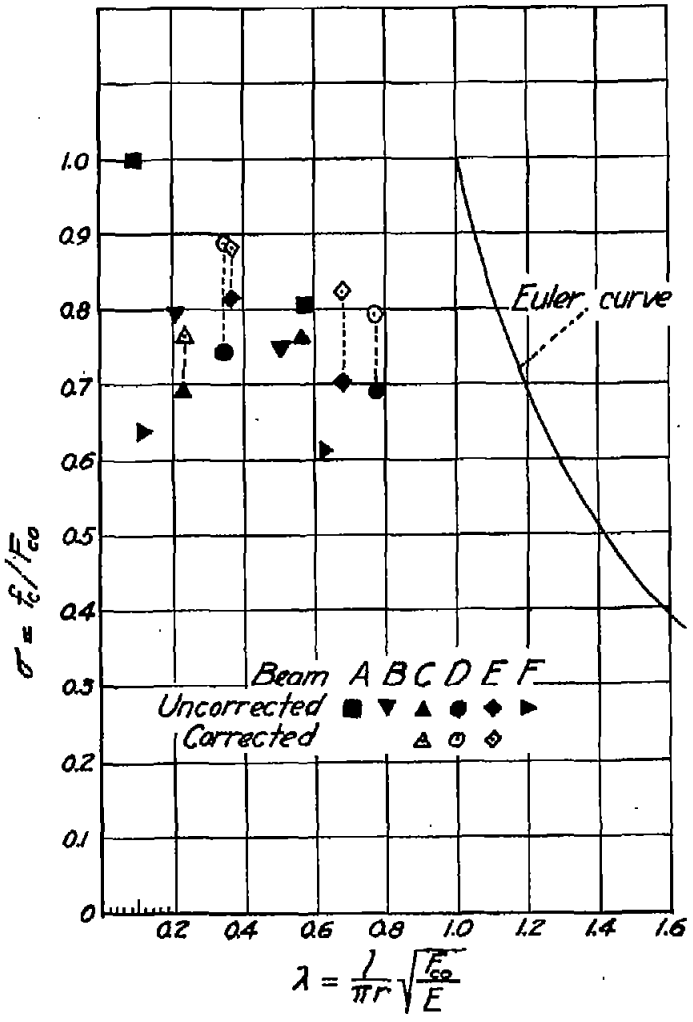

Fig. 19—Effect of length on loads at failure for column specimens 1 and 2

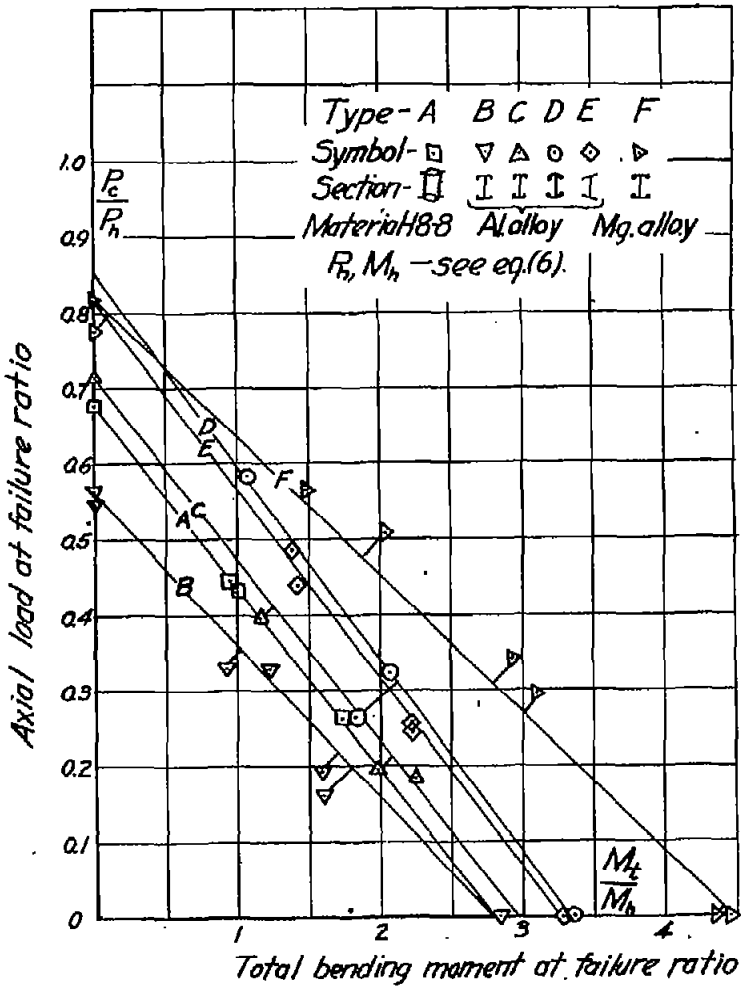

Combined axial load and bending moment on non-dimensional basis.

Fig. 20.

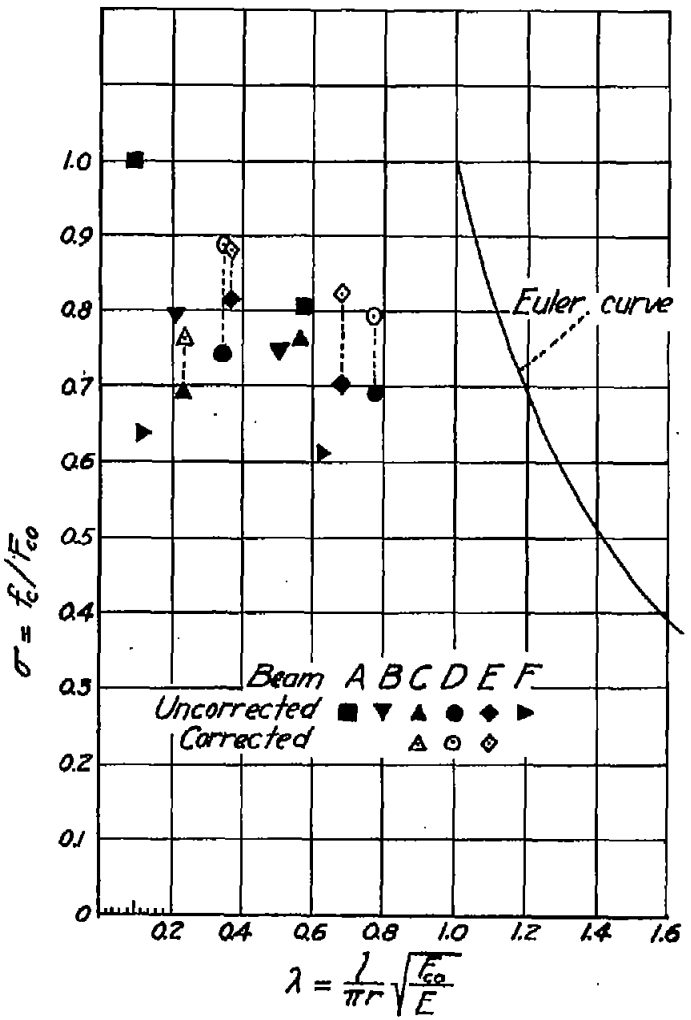

Fig. 19—Effect of length on loads at failure for column specimens 1 and 2

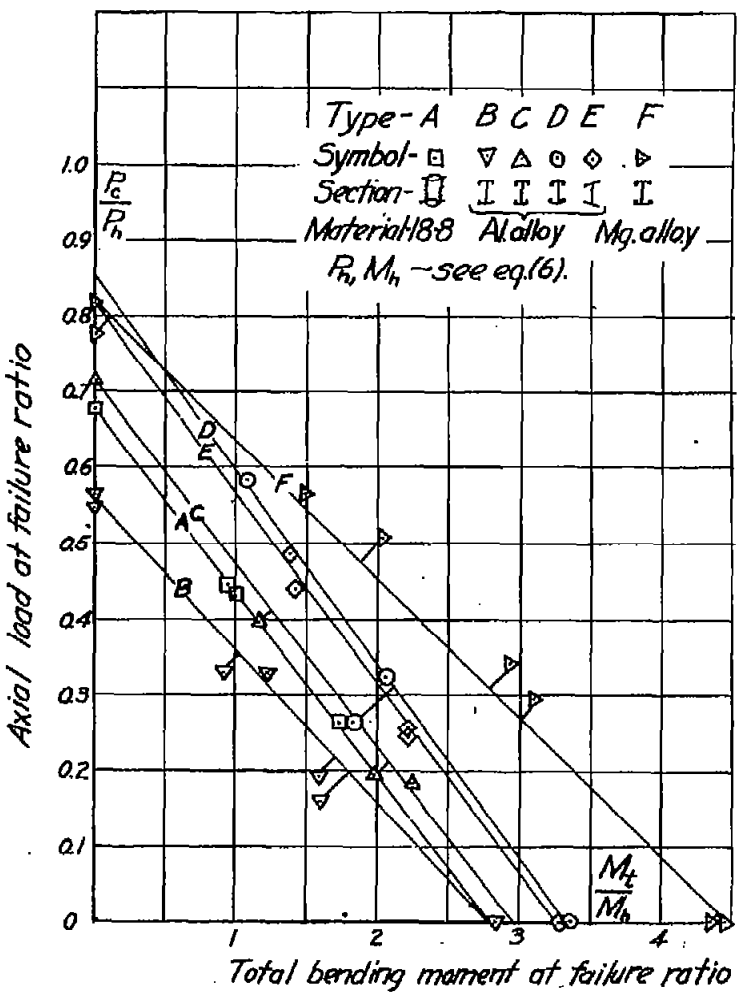

Fig. 20. Combined axial load and bending moment on non-dimensional basis.

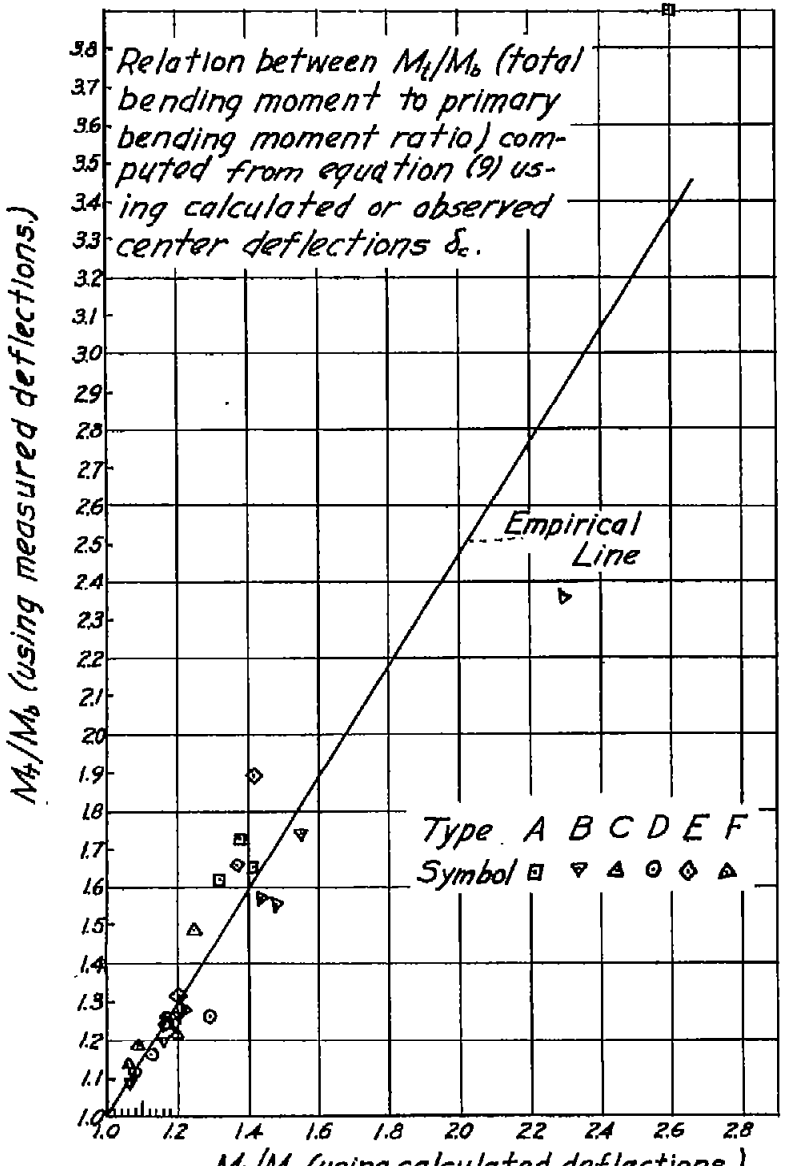
Relation between M_t/M_b (total bending moment to primary bending moment ratio) computed from equation (9) using calculated or observed center deflections δ_c.
Empirical Line
Type A B C D E F
Symbol
M_t/M_b (using measured deflections.)
M_t/M_b (using calculated deflections.)

Fig. 21.

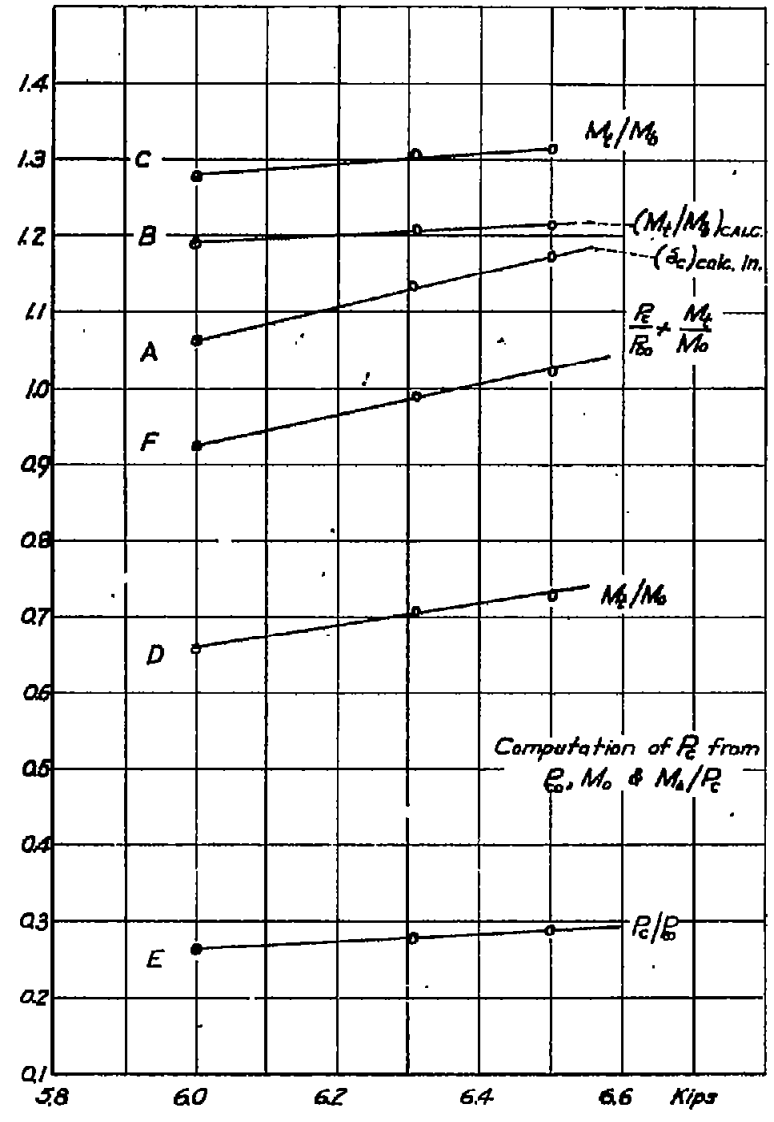
M_t/M_b
$(M_t/M_b)_{calc.}$
$(\delta_c)_{calc.\ in.}$
$\frac{P_c}{P_{co}} + \frac{M_t}{M_o}$
M_o/M_b
Computation of P_c from P_{co}, M_o & M_o/P_c
P_c/P_{co}
A
B
C
D
E
F
P_c
Kips

Fig. 22.